



HAL
open science

Determination of the spectroscopic properties of indium bromide

H C J Mulders, M Haverlag, G M W Kroesen

► **To cite this version:**

H C J Mulders, M Haverlag, G M W Kroesen. Determination of the spectroscopic properties of indium bromide. *Journal of Physics B: Atomic, Molecular and Optical Physics*, 2011, 44 (14), pp.145101. 10.1088/0953-4075/44/14/145101 . hal-00636641

HAL Id: hal-00636641

<https://hal.science/hal-00636641>

Submitted on 28 Oct 2011

HAL is a multi-disciplinary open access archive for the deposit and dissemination of scientific research documents, whether they are published or not. The documents may come from teaching and research institutions in France or abroad, or from public or private research centers.

L'archive ouverte pluridisciplinaire **HAL**, est destinée au dépôt et à la diffusion de documents scientifiques de niveau recherche, publiés ou non, émanant des établissements d'enseignement et de recherche français ou étrangers, des laboratoires publics ou privés.

Determination of Spectroscopic Properties of Indium Bromide

H.C.J. Mulders¹, M. Haverlag^{1,2}, G.M.W. Kroesen¹

¹Department of Physics, Eindhoven University of Technology, P.O.Box 513, 5600MB Eindhoven, The Netherlands

²LightLabs, Koninklijke Philips Electronics N.V., Mathildelaan 1, 5611BD, Eindhoven, The Netherlands

E-mail: h.c.j.mulders@tue.nl

Abstract.

To develop a more efficient plasma light source, molecules are considered as the prime source of radiation, because they can potentially avoid the conversion losses of the low pressure mercury lamp as well as the thermal losses of the high pressure mercury lamps. A candidate to serve as the prime radiator in such a lamp could be Indium Bromide, but spectroscopic data to assess its aptitude is largely unavailable.

To increase the knowledge of the spectroscopic properties of these molecules and InBr in particular, an experiment was designed to acquire this information. Laser Induced Fluorescence was used to study the radiative properties of InBr for lighting purposes. Using an innovative method to interpret the measured data, DETEX plots, more information can be obtained from the spectra. Also the effect of a background gas and plasma was investigated for both a capacitive and an inductive plasma.

Mainly the electronic A-state of InBr was investigated. Results include newly identified rotational transitions, vibrational constants, rotational constants for different vibrational levels, band head wave numbers and Franck-Condon factors for various vibrational transitions.

TV9SR8E4TY

1. Introduction

Some of the most efficient light sources —lamps— we know are the fluorescent lamps and the high intensity discharge lamps. The fluorescent lamp has a very efficient efficient mercury discharge that produces UV radiation with an efficiency of around 75% in practical configurations [1], [2]. This radiation is then converted to visible light using fluorescent powders with a relatively poor efficiency caused by the Stokes losses [3], yielding a total efficiency of around 30%.

The high intensity discharge lamps work rather differently. These lamps produce visible light directly from a mercury discharge enriched with some metals, usually in the form of metal halides. The combination of a 5000 K LTE plasma with a relatively cool wall (1200 K), leads to thermal losses and moreover many lines radiate in the IR region. The overall efficiency of these lamps is also around 30–35%.

To try to avoid the losses incurred in the two lamp types described above, a new lamp type is suggested. Basically, the goal is a lighting system that has the best of both worlds: no conversion losses and no IR and heat losses. In reality though, such a lamp will have a bit of both worlds. The discharge will probably produce radiation with a more desirable spectrum than a low pressure mercury discharge, though probably not quite as good as the discharge in a high pressure lamp. Therefore it may well need some limited conversion of the spectrum in phosphors, but then the hope is that the Stokes losses can at least be significantly reduced. The same holds for the heat losses of such a lamp: much better than for a high pressure discharge, but probably not quite as good as for a low pressure discharge. All in all though, this approach can open up possibilities for a more efficient discharge lamp [4], [5], [6], [7], [8].

A promising candidate to serve as the prime radiator in such a lamp is Indium Bromide, but spectroscopic data to assess its aptitude is largely unavailable. To increase the knowledge of the spectroscopic properties of these molecules and InBr in particular, an experiment was designed to acquire this information. Laser Induced Fluorescence was used to study the radiative properties of InBr for lighting purposes. Results include the temperature dependence of the fluorescence decay time, spectroscopic constants and rotational temperature determination from a LIF spectrum.

InBr has interesting properties for plasma lighting applications [9]. It has a high vapor pressure at low temperatures [10], and significant part of the emitted light is emitted in the (near) visible part of the spectrum [11], [12], [13], [14], [4]. In this article, spectrally resolved laser induced fluorescence measurements on indium bromide will be discussed. First we will discuss some theoretical aspects, such as the general properties of the InBr spectrum and the Franck-Condon factors. Then we will describe the method used to carry out the measurements presented later in this article. Finally we will present the results of the measurements and some conclusions.

2. Theory

2.1. Indium Bromide Spectrum

Here, features of the Indium-Bromide spectrum will be discussed [15], [16], [17], [18], [19]. The ground state of InBr is a $^1\Sigma_0^+$ state. The first excited state, (A) is a $^3\Pi_0^+$ state. There is also a B-state, this is a $^3\Pi_1$ state [20], [21], [22], [23]. Together with the metastable $^3\Pi_0^-$ and $^3\Pi_2$ states, they form a triplet state \ddagger which is split due to spin-orbit coupling. The C state is a $^1\Pi$ state. A schematic drawing (not to scale) of the energy levels is shown in figure (1). The wave number of the photons that can be emitted or

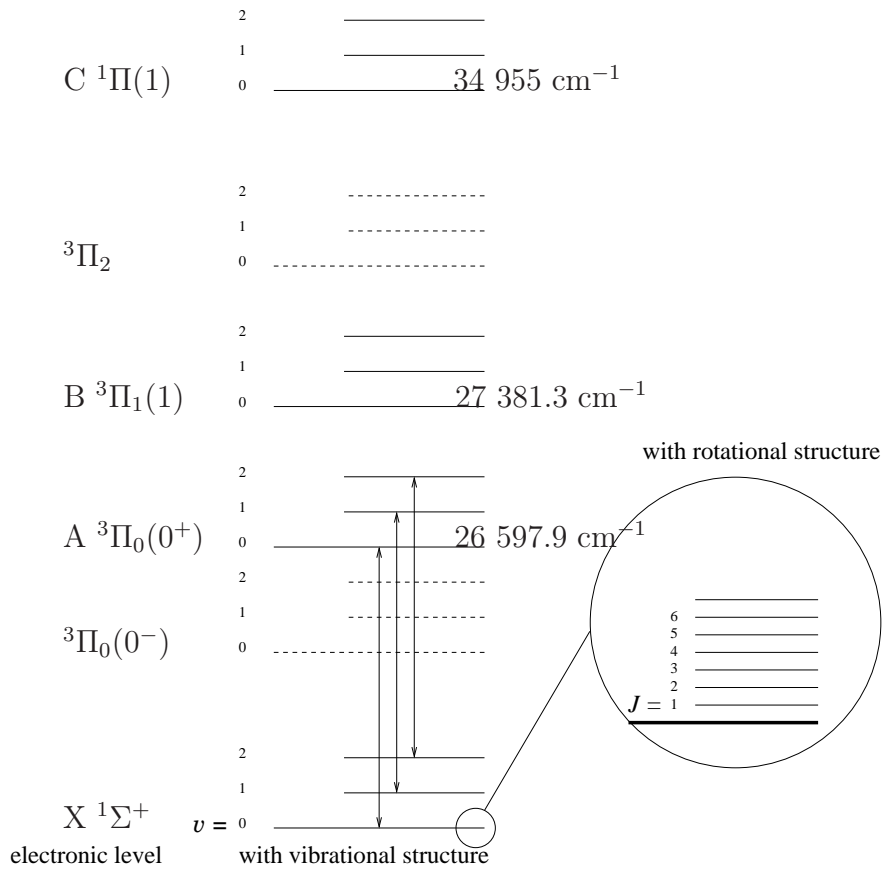


Figure 1. A schematic view of the energy levels of InBr freely after [24]. The electronic states of InBr are shown with three vibration levels each. For the electronic ground state X (vibrational state 0) a schematic drawing of the rotational structure is shown in an inset. All vibrational states of all electronic states of InBr have a rotational structure similar to this one. The dotted lines represent metastable states. The arrows indicate vibrational transitions between the ground state (X) and the A-state with $\Delta v = 0$

absorbed is determined by the difference in energy between the upper and the lower state involved in the transition. In the InBr spectrum, the difference in wave number between

\ddagger It may seem strange that this triplet state consist of four states, however the A ($^3\Pi_0^+$) state and the metastable $^3\Pi_0^-$ are in fact one level split in two states.

transitions that have the same Δv is small§. Therefore, they are grouped together in the spectrum in so called Δv bands. Three of the vibrational transitions that belong to the $\Delta v = 0$ band are shown in figure (1).

An example of the spectrum of an InBr-Argon plasma is shown in figure (2). In this spectrum, the rovibrational structure of the transitions between the electronic A-state and the ground state (X), alongside transitions between the electronic B-state and the ground state (X) can be seen.

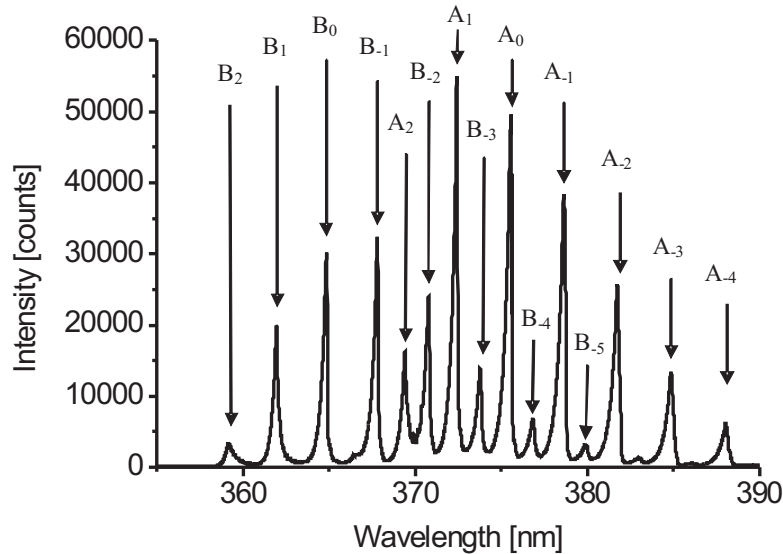


Figure 2. The emission spectrum of an InBr-Argon plasma. The various Δv bands of the electronic A-state and of the electronic B-state are indicated in the figure.

In this article, mainly transitions between the electronic A-state and the ground state are studied. The focus is on the rotational structure of vibrational transitions in the $\Delta v = 0$ band. However, measurements on the $\Delta v = +1$ and $\Delta v = -1$ bands have also been performed. The rotational structure consists of a P-branch, and an R-branch. The P-branch forms a band head. An example of a laser absorption spectrum of the $\Delta v = 0$ band is given in figures (3) and (4). In figure (3) the band heads of the P-branch of the 0-0 and the 1-1 level are indicated. A more detailed view, with the rotational quantum numbers of the levels indicated is shown in figure (4).

Two different stable isotopes of Bromine exist, which are approximately equally naturally abundant: ^{79}Br and ^{81}Br . Therefore, different isotopes of the InBr molecule exist. They are indicated as InBr^{79} and InBr^{81} . For different isotopes, the same general formulae hold, however, the spectroscopic constants such as B_v are (slightly) different.

§ difference in vibrational quantum number ($\Delta v = v' - v''$, where v' denotes the upper and v'' the lower vibrational quantum number.)

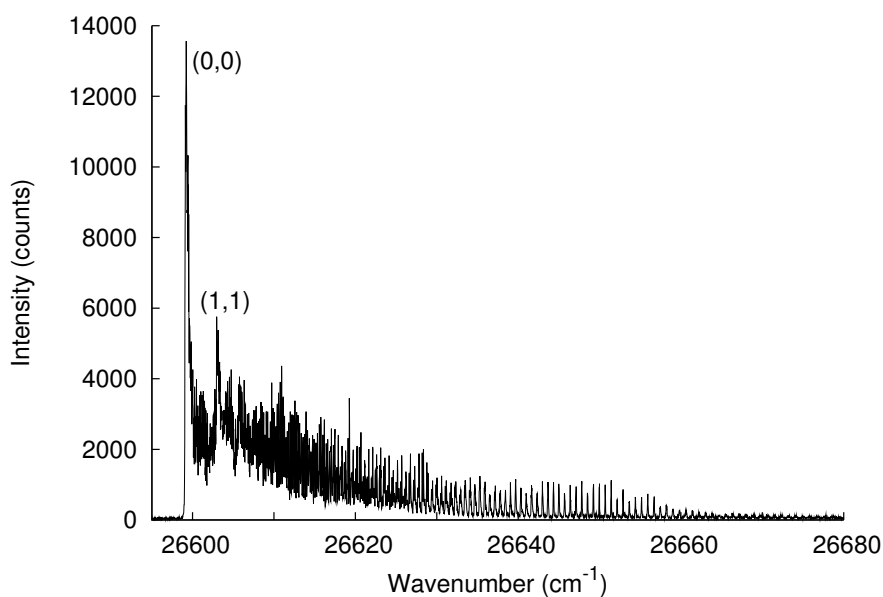


Figure 3. An absorption spectrum of the $\Delta v = 0$ band of the electronic transition between the A-state and the ground state. The band head of the 0-0 and the 1-1 transition are visible on the left. Rotational transitions with higher J are visible to the right. This graph was calculated from a $\Delta v = 0$ DETEX plot by integrating all the fluorescence emission per excitation wavenumber, which corresponds to the absorption at that wavenumber.

2.2. Franck-Condon Factors & Branching Ratios

The vibrational structure of an electronic transition is explained by the Franck-Condon [25] [26] principle as paraphrased by [27]:

Because the nuclei are so much more massive than the electrons, an electronic transition takes place very much faster than the nuclei can respond.

During a transition, *e.g.* from the ground state, the electronic configuration of the molecule is rapidly changed. The nuclei are subjected to a new force field due to the new constellation of electrons around them. They respond by starting to vibrate from their original positions, which was so far unchanged during the rapid electronic transition.

In the quantum mechanical formulation of the Franck-Condon principle, the molecule undergoes a transition to the upper vibrational level that most closely resembles the vibrational wave function of the lower vibrational level of the electronic ground state.

The intensity of a vibronic transition is proportional to the square of the overlap integral between the vibrational wave functions of the two states that are involved in the transition. This is known as the Franck-Condon factor for the transition.

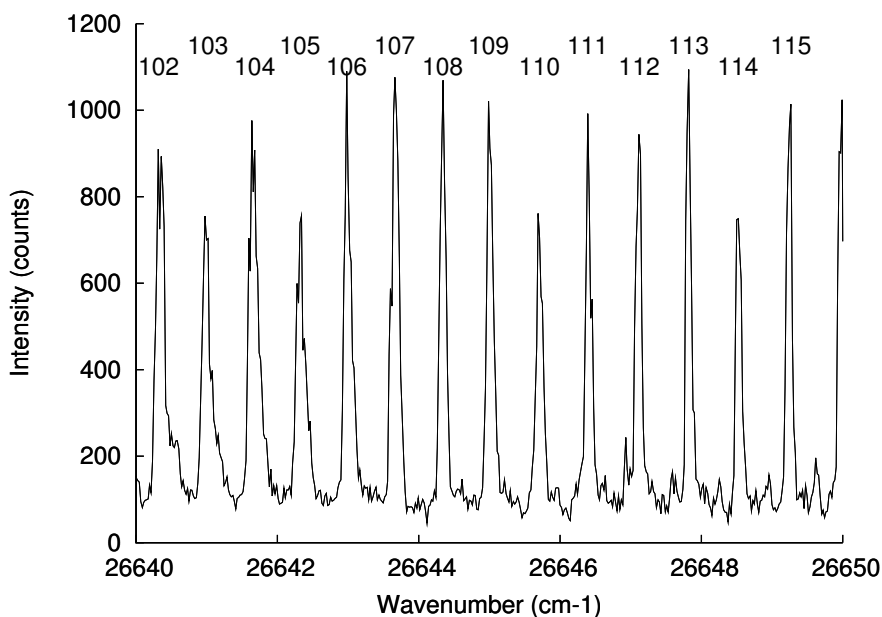


Figure 4. A closer view of the spectrum of figure (3). The big peaks are rotation transitions of the R-branch. In this wave number range the peaks of the P-branch are much less intense. The numbers indicate the rotational quantum number of the ground state of the InBr⁷⁹. To obtain the rotational quantum number of the excited A-state add one, since for the R-branch $J' = J'' + 1$ holds. In this region of the spectrum the rotational quantum number of the R-branch peaks of InBr⁸¹ is one higher than that of InBr⁷⁹, these peaks coincide.

2.3. Rotational Redistribution Broadening

When the InBr molecules collide with Argon atoms, the rotational quantum number can change. It has been observed that for the typical Argon pressures in our experiments, this process can be as fast as the optical decay. The rotational redistribution process becomes faster at higher temperatures, due to the increased collision frequency.

Evidence for the redistribution can be found in the measurements presented further on in this paper. The spectra with Argon as a background gas look distinctly broader than the spectra without background gas. The various aspects of these measurements will be discussed in more detail in section 5.

3. Experimental Setup

3.1. Introduction

A setup was built to perform LIF experiments [28] to determine various fundamental properties of Indium Bromide as well as some operating properties of the lamps under investigation. The gas temperature of these plasmas was one of the most important properties to be measured, as it carries a lot of information about the state of the discharge.

Furthermore, the Franck Condon factors of various vibrational transitions and the corresponding transition energies were determined. Also the transition energies of some rotational transitions were measured.

3.2. General

In this section we will give a general description of the setup. The setup is built around an oven with inside it a quartz tube containing Indium Bromide. The tube containing the InBr is heated to the desired temperature to evaporate the InBr. A laser system is used to excite the molecules. An elaborate detection system containing an iCCD camera and photon counting equipment is used to detect the fluorescence.

3.3. Oven

For the experiment on InBr vapor, the quartz tube with InBr vapor is placed in an oven. In this oven the sample can be heated up to approximately 633 K. However, most of the measurements were done at a temperature of about 513 K to reach the optimal InBr vapor pressure (~ 1 Pa) for the determination of spectroscopic constants in our setup. A higher temperature quickly leads to a much higher pressure causing undesirable broadening of the spectra and at a lower temperature the intensity of the fluorescence quickly drops below the detectable level.

The oven is mounted on two rails that allow for horizontal movement, perpendicular to the axis of the quartz tube inside it. The position is adjusted by moving the micrometer adjuster screw (1 in figure 5). To prevent turbulence in the optical path accessing the oven, two 20 cm long tubes (2 in figure 5) are mounted on both ends of the oven.

Around the oven a heat shield is mounted (3 in figure 5). It also serves as a radiation shield, since the discharge inside can produce UV-radiation. The oven is suspended from 3 rods (4 in figure 5) that connect it to the baseframe. The rods are connected to the quartz part of the oven. The purpose of this construction is to reduce heat conduction losses to the base and optical table.

The oven is heated by six infrared radiators (5 in figure 5): three mounted above the quartz tube and three mounted below the quartz tube. Each group of three heaters is controlled by a separate 2132 Eurotherm PID controller. Each controller is fed with temperature data from a K-thermocouple strategically placed above or below the quartz tube.

The front and back ends of the oven are also heated to create a temperature profile that is as homogeneous as possible. The edge heaters are controlled by one Eurotherm 2116 PID controller. This controller receives temperature data from 2 K-thermocouples attached to the ends of the oven.

After enough stabilization time, the temperature of the oven is within 1 K of the requested temperature. The cold spot of the tube is within 1 K of the oven temperature.

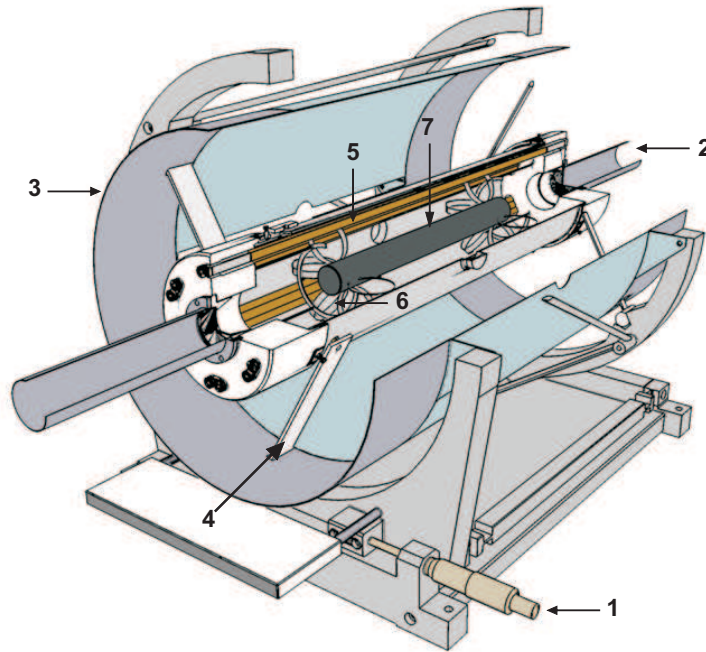


Figure 5. A drawing of the oven with the quartz tube visible inside. 1. Micrometer adjuster screw. 2. Anti-turbulence tubes. 3. Heat shield. 4. Suspension rods. 5. Infrared radiators. 6. Clamping rings. 7. Quartz tube.

6 steel rings (6 in figure 5) hold the quartz tube (7 in figure 5), that will be described in the following section, in place by clamping it firmly. They are flexible, to allow for variation of the tube diameter.

3.4. Quartz Tube

The quartz tube used in this experiment is mounted inside the oven described in section 3.3 as can be seen in figure 5. The tube is about 30 cm long and has a diameter of 3 cm. A small protrusion can be seen at about $\frac{1}{4}$ of the length. This is the pipe that was used to fill the tube with the desired dose and seal it. On the ends of the tube, Tantalum electrodes are used to increase the RF coupling efficiency.

3.5. Excitation

The excitation in this setup is performed by a tunable dye laser pumped by a high repetition rate, frequency tripled Nd:Yag laser, built by EdgeWave GmbH. The laser beam is *not* focussed into the plasma.

The dye laser used in these experiments is a Cobra Stretch high repetition rate laser, manufactured by Sirah GmbH.

The laser dye used in the experiments is Exalite 376, which can emit in the 370—380 nm wavelength range ($\approx 27.0 \cdot 10^3 \text{ cm}^{-1} - 26.3 \cdot 10^3 \text{ cm}^{-1}$). The laser is used to excite the InBr at various wave numbers. In table (1) the specifications of the Nd:Yag

laser and of the dye laser are summarized.

The absolute wavelength error of ≤ 0.03 nm at 570 nm scales to an absolute error of about 1.5 cm^{-1} at 26600 cm^{-1} . The reproducibility of ≤ 0.005 nm at 570 nm scales to an error of about 0.2 cm^{-1} at 26600 cm^{-1} . These specifications indicate the direct tuning to a specific wave number will likely not be very accurate. This is why a laser scan is used. The starting wave number has an offset, but from a starting wave number, the subsequent steps of a scan are reproducible. The shape of the spectrum can be used to calibrate the wave number axis.

Table 1. Properties of the Nd:Yag laser which is used to seed the dye laser

Nd:Yag laser	
wavelength	355 nm
operating current	20 - 40 A
output power	0 - 4 W
pulse duration	5 - 7 ns
repetition rate	1 kHz
dye laser	
grating	3600 lines/mm 90mm
resolution	$3 \cdot 10^6$
absolute wavelength error	≤ 0.03 nm @ 570 nm
wavelength reproducibility	≤ 0.005 nm @ 570 nm
laser dye	
dye	Exalite 376
range	370-380 nm
dye peak efficiency	13%

The high repetition rate is vital for these experiments, due to the easily saturated transitions in this study. To prevent saturation, only very small amounts of energy per shot can be used to induce the fluorescence. This yields very small amounts of fluorescence. In order to detect these signals, the experiment has to be repeated many times. To do this in a reasonable amount of time, a high repetition rate is needed. Experiments were performed to confirm the absence of saturation. The typical modus operandi of these tests was to repeat a measurement with only half the laser power as in the first measurement, then a quarter of the laser power and so on. Without exception, all these tests showed that the signal scaled linearly with the laser power, confirming the absence of saturation.

3.6. Detection

The fluorescence emitted by the excited InBr-molecules is collected with a lens and directed to either a photomultiplier tube (PMT) or an intensified CCD camera (iCCD). A monochromator is used to select the bands for study. Alternatively, a UG11 filter is used to allow light from all A→X and B→X transitions to reach the PMT at once. Using this filter, light from all possible decay paths of the excited level can be detected. The PMT is used to perform the time resolved (tr)-LIF measurements. The iCCD camera is used to perform the spectrally resolved (sr)-LIF measurements.

The monochromator used in this experiment is a Jobin-Yvon HR1000. One of the issues that we encountered with the monochromator was due to temperature stability. The wavelength calibration of the monochromator varied with ambient temperature. This caused undesirable intensity fluctuations in measurements with the PMT resulting in unreliable intensity profiles. The temperature of the lab could vary by more than 10 °C due to the large south facing windows.

To suppress these fluctuations, a system was built to isolate the monochromator from ambient temperature fluctuations. The system was made of an insulating box, a heating device and a feedback control system. This system stabilized the temperature of the monochromator at 40 °C. With this system in place the fluctuations are reduced to an acceptable level of ± 1 pixel from ± 15 pixels. 1 pixel roughly corresponds to 15 pm. Fluctuations up to about 75 pm are acceptable, but anything beyond that creates serious intensity fluctuations in measurements with the PMT.

Observing the LIF signal is not easy because of the low intensity of the light. An iCCD camera was used because it is much more sensitive than a classic CCD camera. The camera used in these experiments is a 4 QuickE iCCD camera made by Stanford Computer Optics. The 4 Quick E camera is fast: it can switch the intensifier on or off in 1.2 ns, making short gating times possible. This is combined with a very high repetition rate (3.3 MHz in burst mode). The spatial resolution of the CCD is 768×494 pixels.

The background level increased problematically during long measurements. This was caused by the increasing temperature of the lab during these measurements.

To decrease the influence of ambient air temperature fluctuations, a water cooled Peltier element is used. It is attached to a heat sink that is directly attached to the CCD matrix.

With this cooling system, a constant temperature of -3 °C is maintained in the iCCD camera. In this way, the background is reduced by a factor ~ 6 , which is essential to make the LIF signal detectable against the background.

The light from the spectrometer is detected with a photomultiplier (PMT) (Hamamatsu H6780) tube to capture and count single photons of one distinct wavelength with good time resolution.

The PMT is connected via an amplifier (Ortec 9306) to an Ortec 9353 multichannel scaler (MCS) to obtain time resolved signals. The MCS has a burst sampling rate of 1 GHz.

A multichannel scaler reacts to a start and a signal pulse. The start pulse starts an internal clock of the MCS that runs from 0 to a preset end time for the experiment. In our experiments, the preset end time is typically of the order of $10\ \mu\text{s}$: the time after which the LIF signal has decayed below the noise level. The detection interval is divided into smaller intervals called bins. The binwidth in our case is typically 1.2 ns.

The signal pulse —sometimes called stop pulse in the instrument jargon— is in our case an amplified pulse from a PMT. If the voltage on the signal port of the MCS increases above an adjustable discriminator level, the MCS detects a pulse. It responds to that by increasing the counter of the appropriate bin by 1. After detecting a pulse, an MCS typically is unable to respond to pulses for some time: the dead time.

By repeating an experiment multiple times, a time evolution of a signal can be gradually acquired this way.

3.7. Plasma

In a number of experiments, a plasma is ignited in the tubes for these experiments. To do this, various RF amplifiers have been used, such as the KALMUS 122C, the Amplifier Research 75A250 and the Electronics & Innovation AB-250. To measure the power going into the plasma, a system of directional couplers was used, made by Amplifier Research. To read out the data from the couplers, the Amplifier Research PM2002 was used.

4. Method: DETEX Plots

The spectrally resolved LIF (sr-LIF) measurements have been performed using the iCCD camera (as described in section 3) to collect the emitted light. Also for these measurements, the dye laser (as described in section 3) is scanned over a preset wave number range. Typically 1000 lasershots are accumulated to produce a camera image. The sr-LIF measurements are time integrated. The time integration frame is $1 \mu\text{s}$. This means that the first $1 \mu\text{s}$ of the fluorescence emission is collected on the iCCD. For each step of the scan, an iCCD image is obtained. The spectral range of one iCCD image is typically about 700 cm^{-1} .

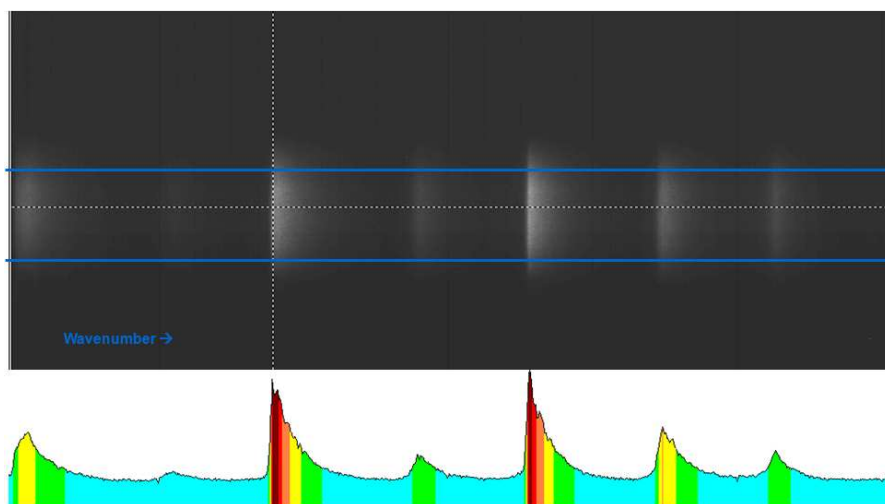


Figure 6. Schematic representation of step 1 in constructing a DETEX plot. For each scan, the energy collected by the camera is plotted as is shown on the bottom of this figure; the detection wave number is put on the horizontal axis. The intensity of the signal is color coded in this frame.

The camera images from all steps in the dye laser scan are combined into a **detection-excitation** plot (DETEX plot). This portmanteau was introduced to abbreviate this word, but also because this is a new diagram to be used in the interpretation of laser induced fluorescence. Similar diagrams have been used for Raman scattering on carbon nanotubes [29].

In these DETEX plots, the excitation wave number is put on the vertical axis. The detection wave number is put on the horizontal axis. The intensity of the detected signal is plotted color coded in this frame, so the color at an x-y coordinate gives the intensity of the emission at the detection wave number (on the horizontal axis) after absorption at the excitation wave number (displayed on the vertical axis). In figure 6 the color coding process is schematically shown. Figure 7 shows a complete DETEX plot.

Putting the detection wave number on the horizontal axis may seem counter intuitive, but it is helpful, because then every horizontal line in the DETEX plot represents a fluorescence spectrum taken at the wave number indicated on the vertical axis.

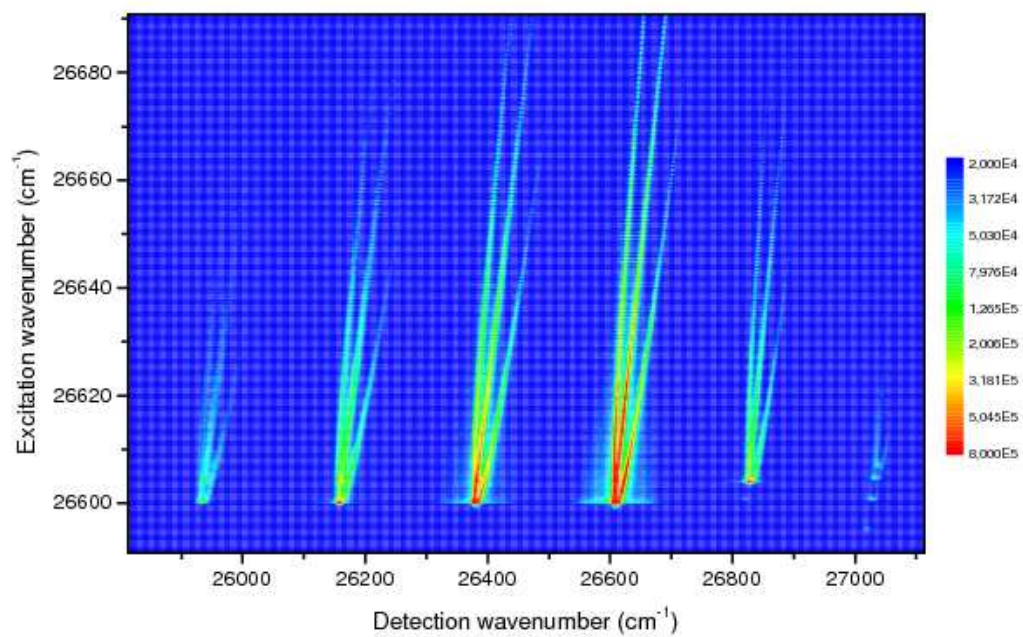


Figure 7. Example of a DETEX plot. The intensity of the measured spectrum is color coded for each x-y-coordinate.

5. Results

In this section the results of the measurements will be shown and discussed. First, results for the InBr vapor *without* buffer gas and without a plasma will be shown, followed by results for the vapor *with* the buffer gas without plasma. Finally results for the plasma will be shown, both for a capacitively coupled plasma and an inductively coupled plasma.

5.1. InBr Vapor DETEX Plots

Figure 8 shows the DETEX plot of the measurement carried out in InBr vapor without background gas and without plasma. In these plots, the sr-LIF signal is shown with the detection wave number on the horizontal axis, for different laser wave numbers (vertical axis). The vertical bands are the various Δv bands. For the InBr measurement, each of them consists of three smaller branches. For these measurements, the laser excitation was in the $\Delta v = 0$ band.

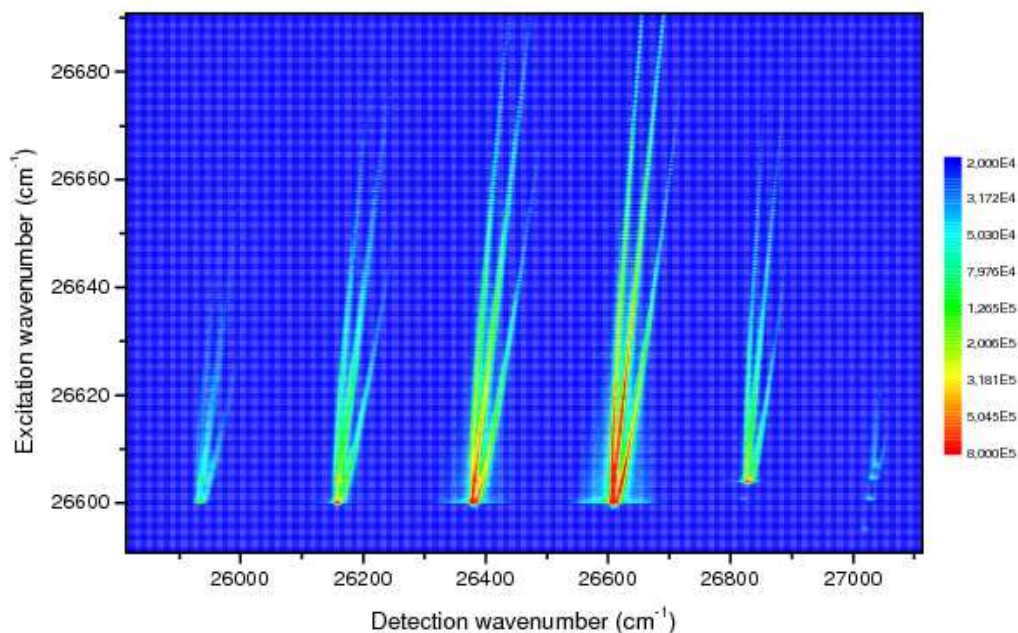


Figure 8. The DETEX plot of the sr-LIF measurement on InBr. Excitation was in the $\Delta v = 0$ band. From left to right the bands $\Delta v = -3$ through $\Delta v = +2$ are shown. Each vibration band consists of three different branches that are explained by the different combinations of rotational transitions in the P-branch and R-branch for excitation and detection.

The vibration bands of the DETEX plots of the InBr measurement show three branches. When the branches are studied carefully, one can see a spot in the central branch for every spot in the left branch, as well as one for every spot in the right branch. This is shown in figure 9.

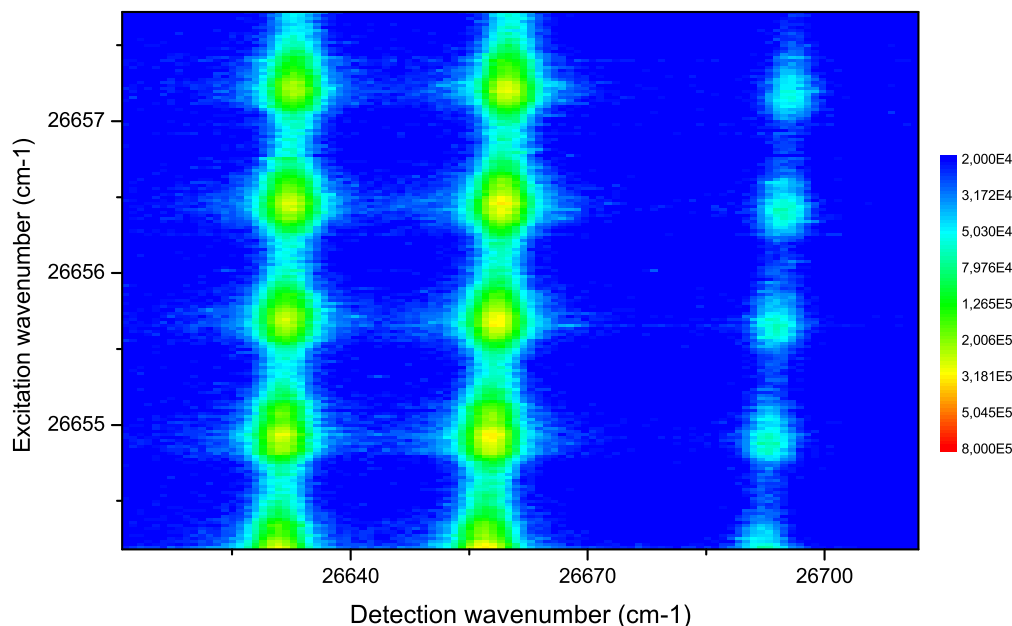


Figure 9. A close up of the DETEX plot of the sr-LIF measurement on InBr. On further inspection of the dots visible in this plot, one can see that the left and right dots do not coincide completely, although they do overlap largely.

This phenomenon is explained by the following. When the laser is tuned to a wave number that matches absorption in the P-branch ($\Delta J = -1$) —*e.g.* between the ground state vibrational level 0, $J=130$ to the excited A-state, vibrational level 0, $J=129$ —, there are two possibilities to go back to the electronic ground state vibrational level 0: to $J=130$, P-branch emission and to $J=128$, R-branch ($\Delta J = +1$) emission. Because the energy difference between (A,0,129)|| and (X,0,130) is smaller than the energy difference between (A,0,129) and (X,0,128), this emission appears on the high wave number side.

Near these lines, there is also excitation via the R-branch, *e.g.* from electronic ground state vibrational level 0, $J=86$ to the excited A-state, vibrational level 0 $J=87$. Also for this excited level, there are two possibilities to go back to the electronic ground state vibrational level 0: to $J=86$, R-branch emission and to $J=88$, P-branch emission. Because the energy difference between (A,0,87) and (X,0,86) is bigger than the energy difference between (A,0,87) and (X,0,88), this emission appears on the low wave number side.

The central branch consists of emissions from relaxation transitions from upper to lower level that take place through the same path as the excitation. The left branch is emission in the R-branch after absorption in the P-branch. The right branch is emission in the P-branch after absorption in the R-branch. In figure (10) an energy level diagram is shown to illustrate this process. In terms similar to the terminology used for selection

|| This is an ad hoc abbreviation for electronic A-state, vibrational level 0, rotational level 129.

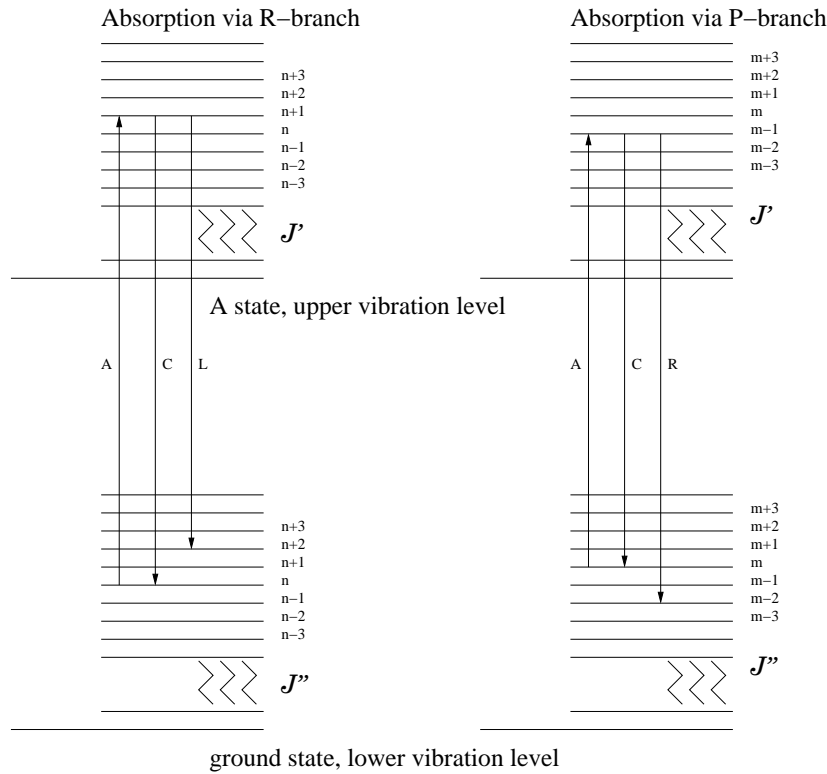


Figure 10. Illustration of the three branches. The letter A stands for absorption, the letters L, C, R indicate that the emitted light is detected in the left, center or right branch of the DETEX plot.

Left: Excitation via the R-branch. Relaxation is possible through two paths, in the R-branch, with the same wave number as the excitation, and in the P-branch, with a lower wave number than the excitation.

Right: Excitation via the P-branch. Relaxation is possible through two paths, in the P-branch, with the same wave number as the excitation and in the R-branch, with a higher wave number.

rules, $\Delta J'' = +2, 0, -2$ can be used to indicate the left (lower detection wave number) central and right (higher detection wave number) branch respectively.

From this explanation it can be concluded that the distance between the left branch and the central branch can be calculated from $F(J'' + 2) - F(J'')$. The distance between the right branch and the central branch follows from $F(J'') - F(J'' - 2)$. Also, the other way around, if the rotational constants of the lower level are known *e.g.* from microwave studies, the distance between the branches can be used to determine the rotational quantum number of the level, though this would require a greater resolution than what is available in our setup.

When the rotational quantum numbers of the upper level and their peak positions are known, the rotational constants of the upper level can be determined from the distance between them. This is done as follows; two peaks with the same lower level are searched, the distance between them is now determined by the rotational constants of the upper level by a formula analogous to the previously mentioned ones.

5.1.1. *Determining wave numbers of rotational transitions of the P-branch $\Delta v = 0$*
 The sr-LIF measurements can be used to determine the rotational quantum number and the wave number of the transitions. For the electronic A-state vibration 0 to the electronic X-state vibration 0 a list of the wave numbers at which different rotations of the P and R-branch appear has been produced by [23]. For high wave numbers, the rotational quantum number of a P-branch transition is approximately 40 higher than the rotational quantum number of an R-branch transition that appears near the same wave number. This is due to fact that the P-branch forms a band head. Because the rotational quantum number of the R-branch is lower, the transitions are more intense. It is therefore difficult to determine the locations of the P-branch transitions for high wave numbers.

From the discussion in the previous section it is concluded that in the DETEX plots, the left rotation branch is light that is emitted in the R-branch after absorption in the P-branch. In this branch, there is no emission from absorption in the R-branch. Therefore, the left rotation branch can be used to determine the wave number of transitions of the P-branch.

To do this, the range of data corresponding to the P-branch under investigation has to be identified and isolated. This is done by carefully selecting the part of the DETEX plot (generally 9 data points wide) and creating a graph of the fluorescence emission of the $v = 0$ P-branch emission of the electronic A-state versus the excitation wavelength. Typically, such a graph looks like an absorption spectrum such as in figure 3, but it exclusively contains emission from the P-branch. After this, the job of identifying peaks and noting their wave number begins (see figure 4). This procedure, produces a list of wave numbers of a sequence of peaks. To find the corresponding rotation quantum number J , it has to be matched with the list produced by [23] —in this case— and for any additional lines, the numbering is continued.

In this article the wave numbers of P-branch transitions have been determined up to $J=174$, which extends the list produced by [23] that goes up to $J=140$. The results are listed in table 2.

Table 2: Identification of the P-branch rotational transitions of the transition between the electronic A-state vibration 0 and the ground state vibration 0 for InBr⁷⁹ and InBr⁸¹

J	InBr ⁷⁹ (cm ⁻¹)	[23] (cm ⁻¹)	InBr ⁸¹ (cm ⁻¹)	[23] (cm ⁻¹)
121	26625.62	26625.59	26625.25	26625.23
122	26.16	26.12	25.77	25.75
123	26.72	26.65	26.30	26.29
124	27.25	27.19	26.84	26.80
125	27.79	27.73	27.38	27.32
126	28.35	28.28	27.93	27.88

127	28.88	28.83	28.47	28.44
128	29.46	29.39	29.03	28.99
129	30.02	29.96	29.61	29.55
130	30.62	30.53	30.14	30.10
131	31.20	31.10	30.72	30.72
132	31.75	31.68	31.30	31.26
133	32.35	32.27	31.81	31.82
134	32.93	32.86	32.35	32.39
135	33.55	33.45	32.93	32.99
136	34.15		33.55	33.57
137	34.75		34.15	34.17
138	35.35		34.75	34.79
139	35.99		35.35	35.39
140	36.62		35.99	36.02
141	37.25		36.62	
142	37.88		37.25	
143	38.55		37.88	
144	39.17		38.55	
145	39.81		39.17	
146	40.47		39.81	
147	41.15		40.47	
148	41.77		41.15	
149	42.47		41.77	
150	43.13		42.47	
151	43.79		43.13	
152	44.50		43.79	
153	45.18		44.50	
154	45.90		45.18	
155	46.59		45.90	
156	47.27		46.59	
157	47.97		47.27	
158	48.70		47.97	
159	49.42		48.70	
160	50.12		49.42	
161	50.87		50.12	
162	51.59		50.87	
163	52.34		51.59	
164	53.06		52.34	
165	53.80		53.06	
166	54.59		53.80	

Table 3. The relative intensities calculated from the data in [21] in the $\Delta v = 1$ band in a DETEX *plot*, after excitation in the $\Delta v = 0$ band at $T = 500$ K, scaled to an intensity of 1 for $v' = 1$.

v'	relative intensity
0	-
1	1.00
2	0.08
3	0.02
4	0.10
5	0.10

167	55.34		54.59	
168	56.10		55.34	
169	56.83		56.10	
170	57.63		56.83	
171	58.44		57.63	
172	59.20		58.44	
173	59.99		59.20	
174	60.76		59.99	

In the $\Delta v = 0$ band, the rotational transitions of the electronic A-state vibration 1 to the electronic X-state vibration 1 appear. Because the transition probability of this transition is smaller [21] (see also table 3), and because the population of vibration level 1 is smaller than that of vibration level 0, the intensity of this transition is lower than the intensity of the 0-0 transition. It is difficult to identify the wave numbers of the 1-1 transition in the $\Delta v = 0$ band. However, after excitation in the $\Delta v = 0$ band, the fluorescence signal in the $\Delta v = 1$ band can be evaluated to determine the wave numbers of the rotations of the 1-1 vibrational transition as a function of the rotational quantum number. These values can then be used to determine the rotational constants of vibration 1 of the electronic A- state.

At $T = 500$ K, the expected relative intensities of emission in the $\Delta v = 1$ band after excitation in the $\Delta v = 0$ band for a LIF measurement are displayed in table 3 for the different upper levels.

To determine the rotational constants of vibrational state 1 of the electronic A-state from a normal absorption or emission spectrum, the $\Delta v = 1$ band is evaluated. At $T = 500$ K, the expected relative intensities of emission in the $\Delta v = 1$ band are displayed in table (4).

By comparing tables 3 and 4, it can be concluded that in a DETEX plot with excitation in the $\Delta v = 0$ band, the fluorescence signal in the $\Delta v = 1$ band will have

Table 4. The relative intensities of emission in the $\Delta v = 1$ at $T = 500$ K for a regular emission or absorption spectrum, scaled to an intensity of 1 for $v' = 1$, based on [21].

v'	relative intensity
0	-
1	1.00
2	0.741
3	0.382
4	0.154
5	0.047

less interference from rotations of other upper levels than in an ordinary absorption or emission spectrum of the $\Delta v = 1$ band. Therefore, it will be easier to determine the wave numbers of the transitions from such a LIF experiment.

This same procedure can be used to isolate rotational spectra from different upper levels by choosing the right combination of excitation and detection band. It can be concluded that DETEX plots resulting from LIF measurements are an accurate method to determine the wave numbers of rotational transitions of various upper levels. This is particularly helpful in dense spectra such as the InBr spectrum.

5.1.2. Determining B_{A0} from the R-branch data of the $\Delta v = 0$ transition In the same way as described in the previous section, the wave numbers of transitions in the R-branch of the transition from the A-state, vibrational level 0 to the ground state, vibrational level 0, have been determined. The results are listed in table 5.

Table 5: Wave numbers of the R-branch rotational transitions of the transition between the electronic A-state vibration 0 and the ground state vibration 0 for InBr⁷⁹ according to the measurement in this report and according to [23]

J , R-branch	InBr ⁷⁹ (cm ⁻¹)	[23] (cm ⁻¹)	J , R-branch	InBr ⁷⁹ (cm ⁻¹)	[23] (cm ⁻¹)
0		26600.35	66		19.94
1		0.47	67		20.40
2		0.59	68		20.88
3		0.72	69		21.37
4		0.86	70		21.87
5		1.00	71		22.37
6		1.15	72		22.86
7		1.13	73		23.37
8		1.45	74		23.88
9		1.61	75		24.39

10		1.79	76		24.91
11		1.95	77	26625.46	25.44
12		2.13	78	25.99	25.97
13		2.32	79	26.55	26.51
14		2.51	80	27.09	27.06
15		2.71	81	27.64	27.61
16		2.94	82	28.18	28.16
17		3.09	83	28.74	28.71
18		3.31	84	29.30	29.28
19		3.54	85	29.87	29.84
20		3.75	86	30.43	30.41
21		3.99	87	31.03	31.00
22		4.37	88	31.61	31.58
23		4.61	89	32.21	32.17
24		4.85	90	32.80	32.77
25		5.10	91	33.38	33.38
26		5.36	92	34.00	33.98
27		5.61	93	34.62	34.60
28		5.88	94	35.24	35.24
29		6.14	95	35.86	35.85
30		6.43	96	36.48	36.47
31		6.69	97	37.12	37.10
32		7.00	98	37.76	37.74
33		7.27	99	38.40	38.38
34		7.58	100	39.04	39.02
35		7.88	101	39.72	39.67
36		8.18	102	40.34	40.32
37		8.51	103	41.05	40.98
38		8.82	104	41.73	41.64
39		9.14	105	42.35	42.31
40		9.47	106	43.07	42.99
41		9.81	107	43.75	43.67
42		10.15	108	44.44	44.35
43		10.49	109	45.14	45.03
44		10.84	110	45.82	45.72
45		11.20	111	46.54	46.43
46		11.56	112	47.25	47.13
47		11.93	113	47.95	47.84
48		12.30	114	48.67	48.55
49		12.68	115	49.40	49.27

50		13.06	116	50.12	50.00
51		13.45	117	50.87	50.72
52		13.84	118	51.59	51.46
53		14.24	119	52.36	52.19
54		14.65	120	53.10	52.94
55		15.05	121	53.85	53.69
56		15.47	122	54.61	54.44
57		15.90	123	55.36	55.21
58		16.32	124	56.12	55.97
59		16.75	125	56.89	56.73
60		17.19	126	57.68	57.50
61		17.62	127	58.46	58.27
62		18.08	128	59.21	59.06
63		18.55	129	60.03	59.88
64		19.00	130	60.86	60.68
65		19.46			

Using this information, one can make a graph of J versus wave number for this specific transition. It can then be fitted with a formula describing the relationship between J and the wave number for the R-branch:

$$\begin{aligned} \nu(J) = \nu_0 &+ J^4(D'' - D') \\ &+ J^3(2D'' - 6D') + J^2(-B'' + B' + D'' - 13D') \\ &+ J(-B'' + 3B' - 12D') + 2B' - 4D'. \end{aligned} \quad (1)$$

In this equation, $\nu(J)$ denotes the wave number of the R-branch transition for that particular rotational quantum number J . ν_0 is the wave number of the vibronic transition (incorporating the electronic and vibrational transition energy). B is the rotational constant where a single prime denotes the *upper* state and a double prime the *lower* state.

This aforementioned graph for the most comprehensive data set we have, which is from [23] up to $J = 76$ and data from our own measurement up to $J = 130$, is presented in figure 11. The R-branch data is fitted with equation 1. From microwave measurements [23] it is known that the ground state rotational constant $B'' = 0.0557099 \text{ cm}^{-1}$ and the ground state anharmonicity $D'' = 1.42 \cdot 10^{-8} \text{ cm}^{-1}$. From the fit various constants were determined: the rotational constant of the lowest vibrational level of the A-state $B' = B_{A0} = 0.058410 \pm 0.000002 \text{ cm}^{-1}$ and the anharmonicity $D' = D_{A0} = 1.59 \cdot 10^{-8} \pm 1 \cdot 10^{-10} \text{ cm}^{-1}$.

To check the consistency, also the P-branch data was fitted. The values found were $B' = B_{A0} = 0.05842 \pm 0.00001 \text{ cm}^{-1}$ and $D' = D_{A0} = 1.55 \cdot 10^{-8} \pm 5 \cdot 10^{-10} \text{ cm}^{-1}$. These

results are consistent with the data presented above, however less accurate, due to the smaller and noisier data set.

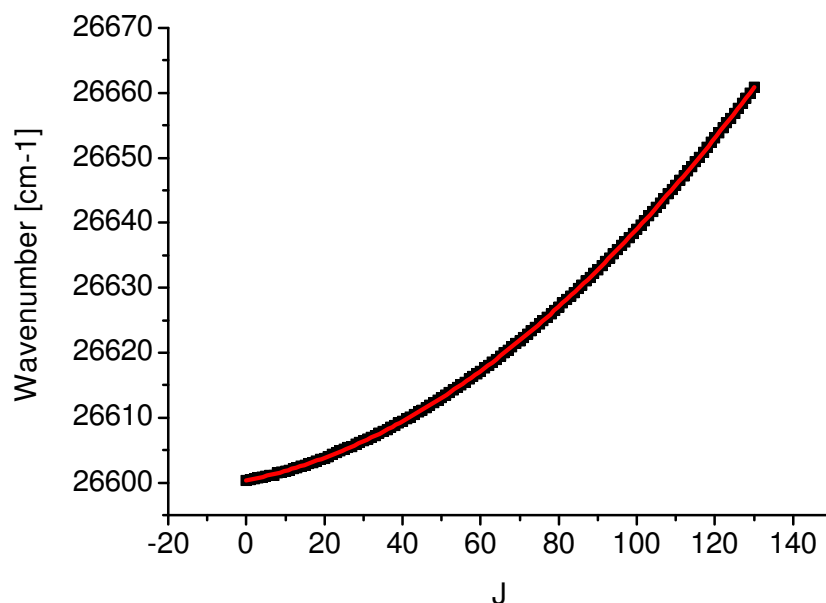


Figure 11. Graph of wave number versus rotational quantum number for the R-branch of the 0-0 transition from the A-state to the ground state. The red line running through the data points is a fit based on 1

5.1.3. *Determining B_{A1} from the R-branch data of the $\Delta v = 1$ transition* To determine the rotational constant of the first vibrational level of the A-state (and its anharmonicity), the DETEX plot acquired by exciting in the $\Delta v = +1$ band has to be examined. It is shown in figure 12.

After isolating the R-branch of the $\Delta v = +1$ in the data set, a graph of the relative intensity of the R-branch signal versus the wave number is obtained, as is shown in figure 13.

From this graph, the wave numbers of the peaks were obtained, resulting in a sequence of identified peaks which are listed in table 6.

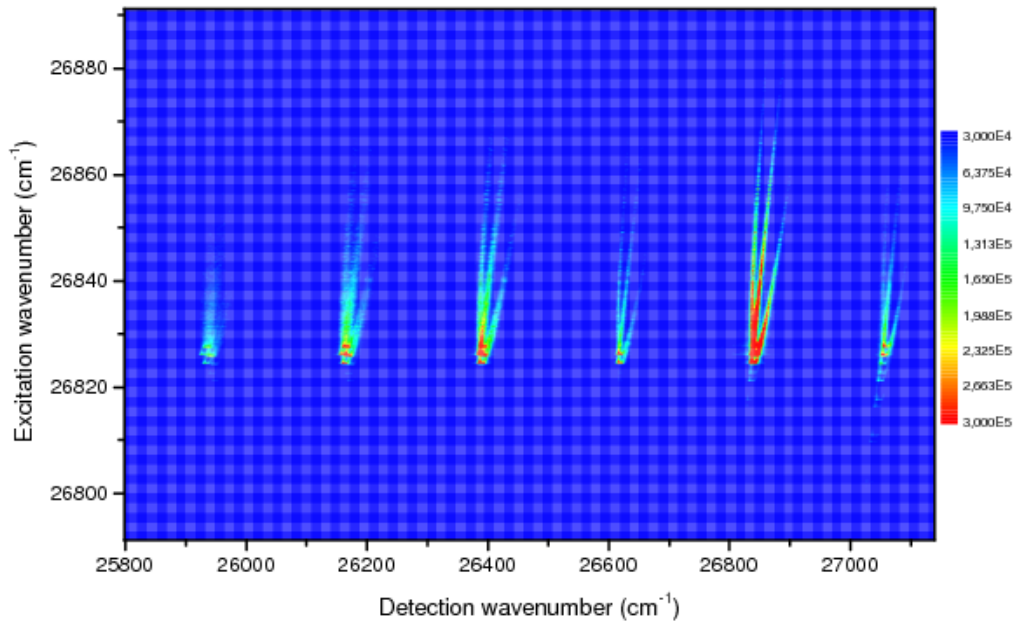


Figure 12. The DETEX plot of the sr-LIF measurement on InBr. Excitation was in the $\Delta v = +1$ band. From left to right the bands $\Delta v = -3$ through $\Delta v = +2$ are shown. Each vibration band consists of three different branches that are explained by the different combinations of rotational transitions in the P-branch and R-branch for excitation and detection.

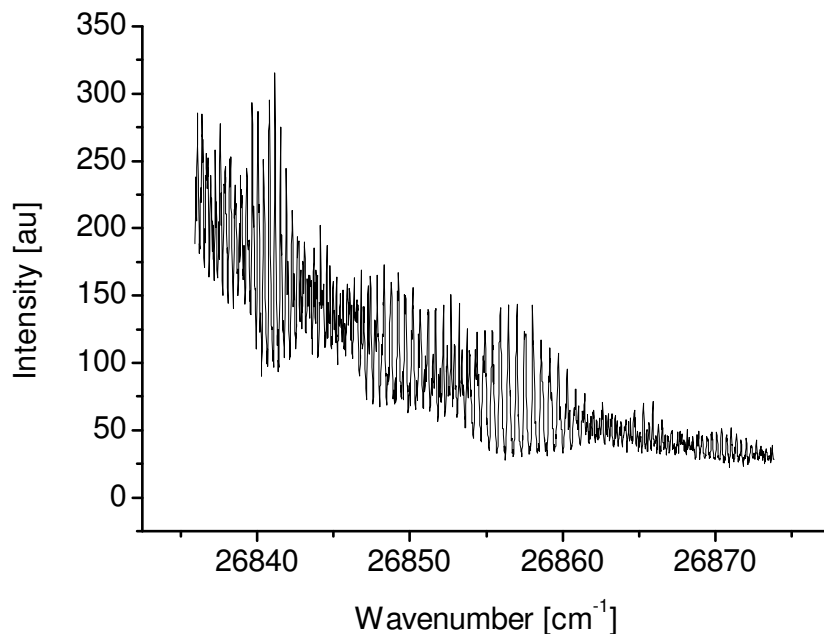


Figure 13. Graph of the intensity of the R-branch of the $\Delta v = +1$ vibrational transition versus the wave number versus at which it occurred.

Table 6: Wave numbers of the R-branch rotational transitions of the transition between the electronic A-state vibration 1 and the ground state vibration 0 for InBr, for both isotopes. Since the assignment of these levels is unknown, they are simply numbered with index i . Note that in the first entry in the table the wave number of the band start is stated. Due to the noise levels, it

i	Isotope 1 (cm^{-1})	Isotope 2 (cm^{-1})	i	Isotope 1 (cm^{-1})	Isotope 2 (cm^{-1})
$J = 0$	26827.78	26827.78	41	51.5223	52.7039
$i = 1$	36.1160	36.1160	42	51.9656	53.2332
2	36.4109	36.4109	43	52.4500	53.7391
3	36.6844	36.6844	44	52.9148	54.2879
4	36.9793	36.9793	45	53.4012	54.7742
5	37.2742	37.2742	46	53.8875	55.3875
6	37.5906	37.5906	47	54.3934	55.9363
7	37.9285	37.9285	48	54.9227	56.4656
8	38.2449	38.2449	49	55.3875	57.0144
9	38.5613	38.5613	50	55.9363	57.5223
10	38.8367	38.9617	51	56.4656	58.0281
11	39.1531	39.3211	52	57.0144	58.5789
12	39.4891	39.6805	53	57.5223	59.2977
13	39.8055	40.0594	54	58.0281	59.825
14	40.1434	40.4188	55	58.5789	60.4598
15	40.4188	40.9871	56	59.1492	61.0301
16	40.8406	41.368	57	59.7195	61.6219
17	41.1766	41.6199	58	60.2898	62.2137
18	41.5574	42.0418	59	60.7406	62.8269
19	41.9168	42.4441	60	61.4539	63.5477
20	42.3172	42.866	61	61.9813	64.1394
21	42.6336	43.2879	62	62.5535	64.6883
22	43.0125	43.7098	63	63.1238	65.0477
23	43.3934	44.1531	64	63.7156	65.6609
24	43.8777	44.575	65	64.3289	66.2547
25	44.3426	44.9754	66	64.6883	66.8680
26	44.7859	45.4671	67	65.2820	67.5242
27	45.2078	45.9051	68	65.8953	68.0105
28	45.6297	46.3699	69	66.4871	68.5184
29	46.0516	46.8133	70	67.1434	69.1316
30	46.5164	47.2762	71	67.6512	69.7664
31	46.9598	47.7195	72	68.1375	70.3797
32	47.4246	48.2273	73	68.8992	71.0144
33	47.8680	48.7762	74	69.4285	71.6492
34	48.3113	49.2625	75	70.0633	72.3484
35	48.7762	49.7254	76	70.7195	
36	49.2625	50.1902	77	71.3738	
37	49.6629	50.6766	78	72.0105	
38	50.1063	51.2039	79	72.6668	

39	50.5711	51.6902			
40	51.0144	52.198			

Due to the noise levels, it can be quite difficult to identify and follow sequences of peaks and in this case the confidence in the accuracy of the first column (Isotope 1) of peaks is higher. Therefore, this column will be used to calculate B_{A1} and D_{A1} . Of course a major obstacle in achieving this goal is the assignment of the rotational quantum number (or lack thereof). To make a best guess —because that is what it will be— the fit with formula 1 is performed for various values of i . The various fitted parameters are evaluated and compared to the values that are expected. This is shown for the wave number of $\nu(0)$, as is shown in figure 14.

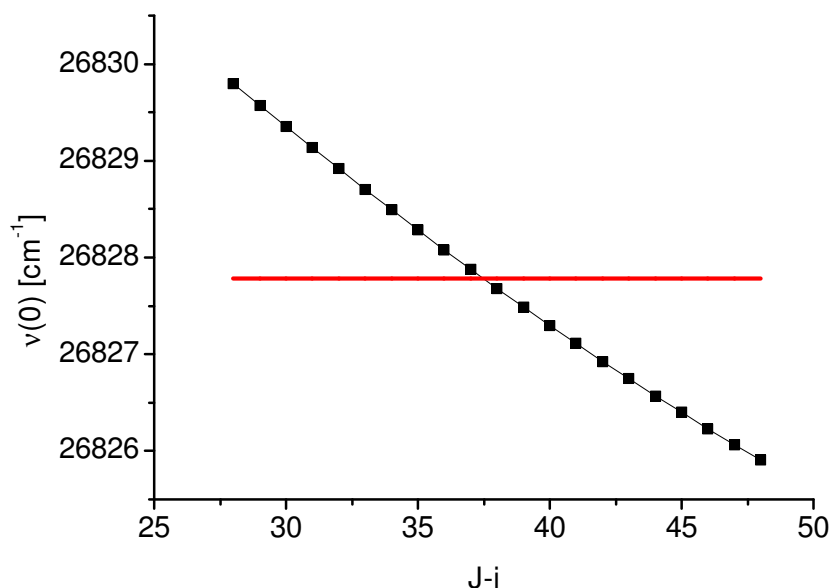


Figure 14. Graph of the wave number of $\nu(0)$ as determined from the fit based on 1 versus various values for $J - i$. The red line running through the data points is the actual $\nu(0)$ as directly measured from the data. The position of the bandhead suggests that $J = i + 38$ provided the best fit.

The same is done for the rotational constant B_{A1} and for D_{A1} .

The best value for $J - i$ is determined by assuming that the value found for the fitted $\nu(0)$ should be close to the measured value. For the values of B_{A1} and D_{A1} it is assumed that they are probably close to the values found for B_{A0} and D_{A0} .

The best fit (for $J = i + 38$) is shown in figure 15. It leads to $B_{A1} = 0.05809 \pm 0.00005 \text{ cm}^{-1}$ and $D_{A1} = 1.8 \cdot 10^{-8} \pm 0.2 \cdot 10^{-8} \text{ cm}^{-1}$. In this case the assignment for J is $J = i + 38$. The uncertainty band of these numbers is determined by the change as a consequence of a mis-assignment of J of ± 1 . This would lead to a relatively small change in B_{A1} , but it would lead to a significant change in D_{A1} of the order of 10%.

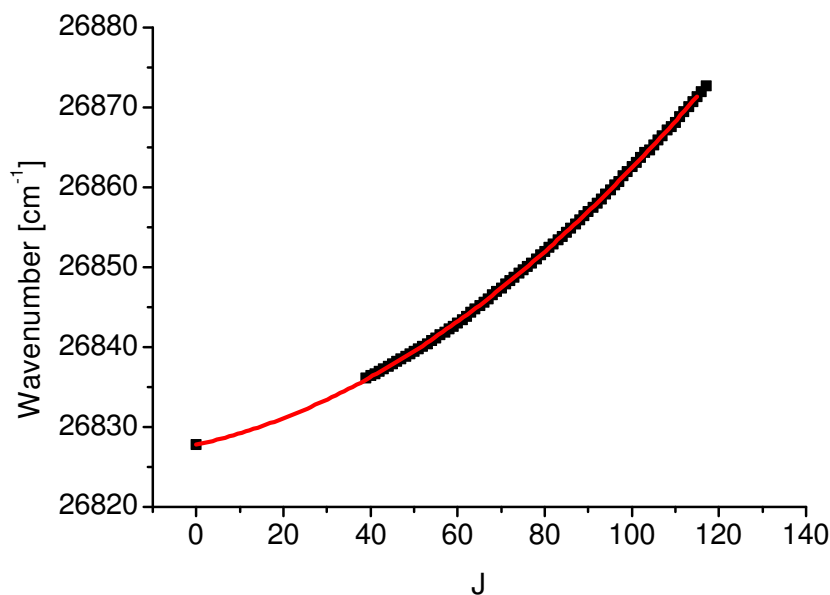


Figure 15. Graph of wave number versus rotational quantum number for the R-branch of the transition from the A-state vibrational level 1 to the ground state vibrational level 0. The red line running through the data points is a fit based on equation 1.

5.1.4. *Determining B_{X1} from the R-branch data of the $\Delta v = -1$ transition* To determine B_{X1} , the first method to be tried was by looking at the DETEX plot obtained by exciting via the $\Delta v = -1$ transition. This plot is shown in figure 16. The problem with this approach is that there are simply too many different vibrational transitions with a high intensity in this particular Δv -branch. This fact makes it virtually impossible to distinguish the individual rotational transitions on close inspection, because there are simply too many sets of lines that are mixed together. What would have been nice about this method is that it couples the $v = 1$ level of the electronic ground state with the $v = 0$ level of the A-state, of which the rotational constants are known to a high degree of accuracy.

Another option to obtain B_{X1} is to use the $\Delta v = 0$ DETEX plot as was shown in figure 8. Since B_{A1} was already determined in the previous section, we can use this plot to couple the $v = 1$ level of the ground state with the $v = 1$ level of the A-state.

Just like in the previous section, the applicable set of data is isolated. A graph of the relative intensity of the R-branch signal versus the wavelength is obtained, as is shown in figure 17.

From this graph, the peaks were identified, resulting in a sequence of identified peaks which are tabulated in table 7.

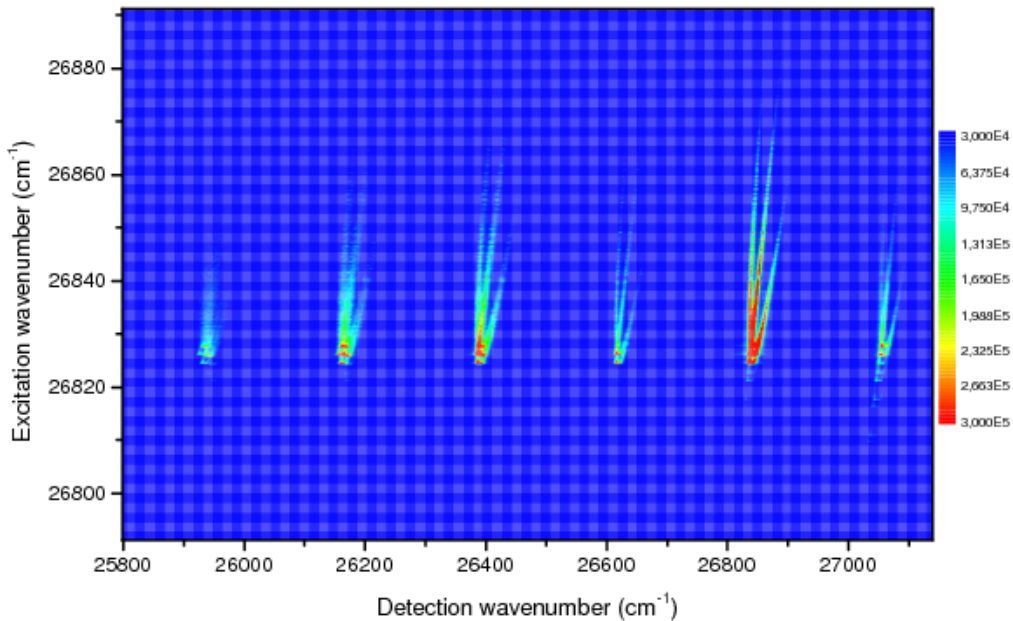


Figure 16. The DETEX plot of the sr-LIF measurement on InBr. Excitation was in the $\Delta v = -1$ band. From left to right the bands $\Delta v = -3$ through $\Delta v = +2$ are shown. Each vibration band consists of three different branches that are explained by the different combinations of rotational transitions in the P-branch and R-branch for excitation and detection.

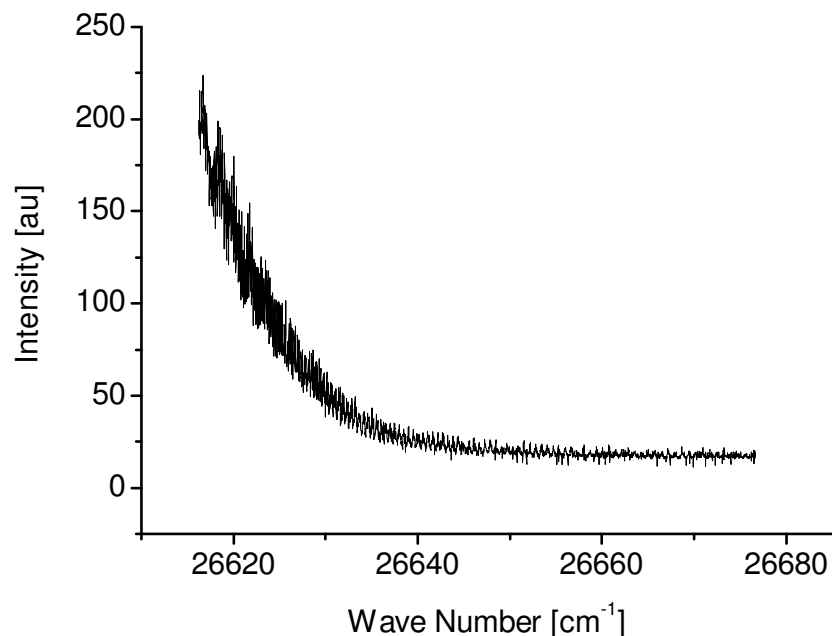


Figure 17. Graph of the intensity of the R-branch of the $\Delta v = +1$ vibrational transition versus the wave number of the fluorescence.

Table 7: Wave numbers of the R-branch rotational transitions of the transition between the electronic A-state vibration 1 and the ground state vibration 1 for InBr, for both isotopes. Since the assignment of these levels is unknown, they are simply numbered with index i . Note that in the first entry of the table is the wave number of the band start. Due to the noise levels, it can

i	Isotope 1 (cm^{-1})	Isotope 2 (cm^{-1})	i	Isotope 1 (cm^{-1})	Isotope 2 (cm^{-1})
$J = 0$	26683.9200	26683.9200	57	38.0059	61.6219
$i = 1$	17.7441	36.1160	58	38.459	62.2137
2	17.9707	36.4109	59	39.0176	62.8269
3	18.1563	36.6844	60	39.4922	63.5477
4	18.4023	36.9793	61	39.9668	64.1394
5	18.6289	37.2742	62	40.5449	64.6883
6	18.8770	37.5906	63	41.0605	65.0477
7	19.1855	37.9285	64	41.6387	65.6609
8	19.3906	38.2449	65	42.1953	66.2547
9	19.6797	38.5613	66	42.6914	66.8680
10	19.9258	38.9617	67	43.2695	67.5242
11	20.2148	39.3211	68	43.8477	68.0105
12	20.4414	39.6805	69	44.3848	68.5184
13	20.7305	40.0594	70	44.9213	69.1316
14	21.0176	40.4188	71	45.5410	69.7664
15	21.2852	40.9871	72	46.1191	70.3797
16	21.5742	41.3680	73	46.6758	71.0144
17	21.8828	41.6199	74	47.2754	71.6492
18	22.1914	42.0418	75	47.8750	72.3484
19	22.5020	42.4441	76	48.4746	
20	22.8105	42.8660	77	49.1348	
21	23.1191	43.2879	78	49.6504	
22	23.4492	43.7098	79	50.3340	
23	23.7578	44.1531	80	50.9121	
24	24.0879	44.5750	81	51.5313	
25	24.4375	44.9754	82	52.1934	
26	24.7676	45.4671	83	52.7930	
27	25.1387	45.9051	84	53.4531	
28	25.4883	46.3699	85	54.0313	
29	25.8398	46.8133	86	54.7344	
30	26.1895	47.2762	87	55.2520	
31	26.5605	47.7195	88	55.9961	
32	26.7512	48.2273	89	56.6777	
33	27.3223	48.7762	90	57.3184	
34	27.7344	49.2625	91	58.0430	
35	28.1055	49.7254	92	58.7461	
36	28.4766	50.1902	93	59.4082	
37	28.8906	50.6766	94	60.0703	
38	29.3027	51.2039	95	60.7520	

39	29.7344	51.6902	96	61.4766	
40	30.1270	52.1980	97	62.1582	
41	30.5391	52.7039	98	62.8613	
42	30.9727	53.2332	99	63.5859	
43	31.4258	53.7391	100	64.2284	
44	31.8379	54.2879	101	65.0137	
45	32.2910	54.7742	102	65.7598	
46	32.7461	55.3875	103	66.4844	
47	33.1777	55.9363	104	67.1465	
48	33.6113	56.4656	105	67.8711	
49	34.1484	57.0144	106	68.6563	
50	34.5820	57.5223	107	69.4238	
51	35.0547	58.0281	108	70.1484	
52	35.5098	58.5789	109	70.9551	
53	35.9844	59.2977	110	71.6798	
54	36.5000	59.8250	111	72.4453	
55	36.9941	60.4598	112	73.2949	
56	37.4492	61.0301			

To make a best guess the fit with formula 1 is performed for various values of i . The various fitted parameters are evaluated and compared to the values that are expected for them. This is done for the wave number of $\nu(0)$, the rotational constant B_{X1} and for D_{X1} .

The best value for $J - i$ is determined by assuming that the value found for the fitted $\nu(0)$ should be close to the measured value. For the values of B_{X1} and D_{X1} it is assumed that they are probably close to the values found for B_{X0} and D_{X0} .

The best fit (for $J = i + 56$) is shown in figure 18. It leads to $B_{X1} = 0.056677 \pm 0.00002 \text{ cm}^{-1}$ and $D_{X1} = 2.83 \cdot 10^{-8} \pm 0.01 \cdot 10^{-8} \text{ cm}^{-1}$. In this case the assignment for J is $J = i + 56$. The uncertainty band of these numbers is determined by the change as a consequence of a mis-assignment of J of ± 1 . This would lead to a relatively small change in B_{X1} and in D_{X1} . The value of D_{X1} is surprising, because it differs significantly from D_{X0} .

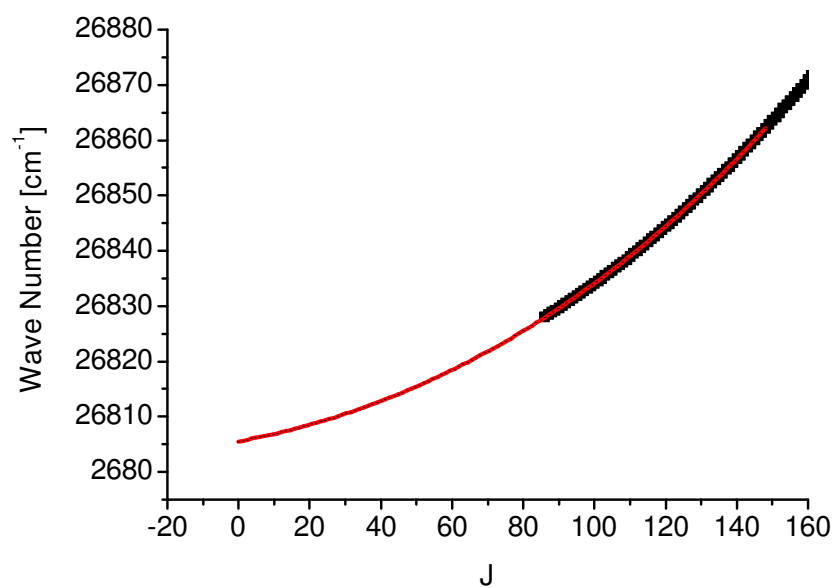


Figure 18. Graph of wave number versus rotational quantum number for the R-branch of the transition from the A-state vibrational level 1 to the ground state vibrational level 1. The red line running through the data points is a fit based on equation 1

5.1.5. *Franck-Condon Factors* Closer inspection of the DETEX plots reveals the data necessary to determine the Franck-Condon factors of various transitions, because for every excitation wave number, a fluorescence spectrum was recorded as was explained earlier. The intensity ratios of the various Δv -bands are a manifestation of the Franck-Condon factors and the population of the (vibrational) level from which the excitation took place.

By looking for an *excitation* wave number that only excites *from* a single vibrational level of the ground state and therefore *to* a single vibrational level of the A-state, it is possible to find a very direct representation of the Franck-Condon factors in the DETEX plots.

For the $v' = 0$ vibrational level of the A-state this was done by looking at the fluorescence spectrum after excitation at 26600 cm^{-1} . At this energy, only excitation from $v'' = 0$ in the ground state to $v = 0$ in the A-state is possible, so all excited molecules are in the $v' = 0$ level of the A-state. By evaluating the fluorescence spectrum taken from the $\Delta v = 0$ DETEX plot (figure 8) as shown in figure 19, it is possible to determine the relative intensities of the different decay paths, which correspond directly to the probability of that specific decay path. This probability is the Franck-Condon factor.

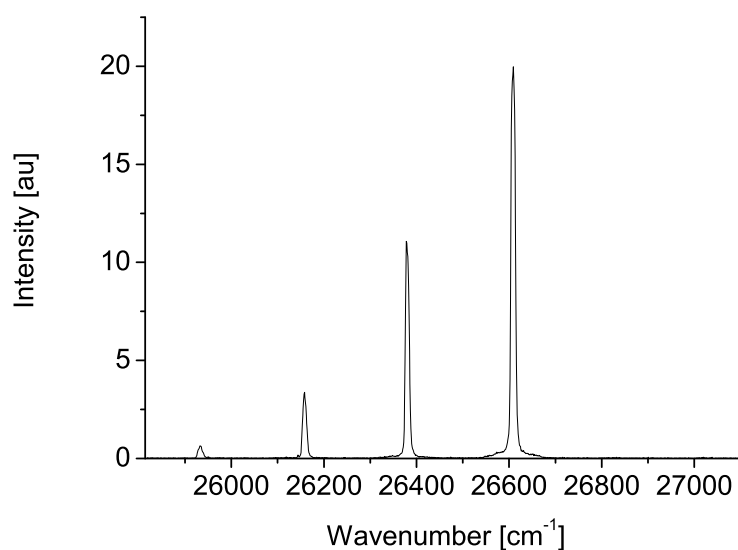


Figure 19. Graph of the fluorescence recorded after excitation at 26600 cm^{-1} . At this wave number, all excited molecules are at $v' = 0$ in the A-state.

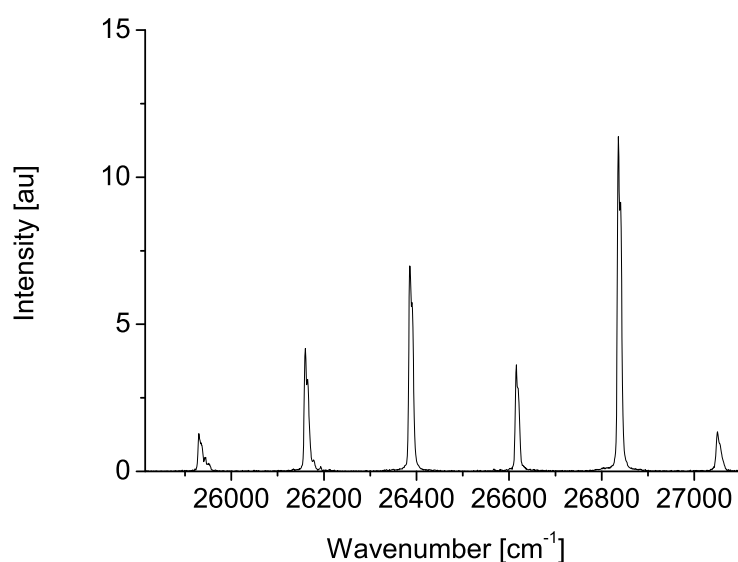
The relative intensities are determined from figure 19 by calculating the total fluorescence emission for each Δv -band by integrating the area under each emission peak and dividing it by the total emission from all Δv -bands. The Franck-Condon factors found this way are listed in table 8.

Table 8. Franck-Condon factors determined from the DETEX plots with excitation via $\Delta v = 0$. Theoretical values from Singh [21] are given for comparison.

	Franck-Condon factor	[21]
$A(v = 0) \rightarrow X(v = 0)$	0.602	0.6030
$A(v = 0) \rightarrow X(v = 1)$	0.289	0.2841
$A(v = 0) \rightarrow X(v = 2)$	0.088	0.0861
$A(v = 0) \rightarrow X(v = 3)$	0.018	0.0211
$A(v = 0) \rightarrow X(v = 4)$		0.0046

The error in these values is estimated to be 2%. That brings the measured values very close to—but not exactly in—agreement with the values found in [21].

The same procedure was followed for the $v' = 1$ level of the A-state. The resulting graph taken at 26825 cm^{-1} from the $\Delta v = 1$ excitation DETEX plot is shown in figure 20.

**Figure 20.** Graph of the fluorescence recorded after excitation at 26825 cm^{-1} . At this wave number, most excited molecules are at $v' = 1$ in the A-state.

The integrated intensities of these peaks are listed in table 10.

An interesting observation is the fact that there is emission visible in the $\Delta v = +2$ -band, since photons emitted in that band can not originate from molecules in the $v' = 1$ level of the A-state. This is caused by higher vibrational transitions, such as the 3-4 and 4-5 transition. This means that a small part of the emission recorded in figure 20 does not originate from the desired $v' = 1$ level. This has consequences for the accuracy of the Franck-Condon factors determined from this data. Since about 5.6% of the emission

Table 9. Relative intensities of each Δv -band as determined from 20.

Fluorescence band	Relative emission
$\Delta v = +2$	0.056
$\Delta v = 0$	0.118
$\Delta v = -1$	0.244
$\Delta v = -2$	0.150
$\Delta v = -3$	0.057

is visible in the $\Delta v = +2$ -band, the margin of error for the Franck-Condon factors found is estimated at 10%. The Franck-Condon factors determined from this data are listed in table 10. Again, the values found in these experiments are close to, but not in exact agreement with the values found in [21].

Table 10. Franck-Condon factors determined from the DETEX plots with excitation via $\Delta v = +1$. Theoretical values from Singh [21] are given for comparison.

	Franck-Condon factor	[21]
$A(v = 1) \rightarrow X(v = 0)$	0.375	0.3273
$A(v = 1) \rightarrow X(v = 1)$	0.118	0.1538
$A(v = 1) \rightarrow X(v = 2)$	0.244	0.2863
$A(v = 1) \rightarrow X(v = 3)$	0.150	0.1562
$A(v = 1) \rightarrow X(v = 4)$	0.057	0.0555

5.1.6. Determination of Band Head Wave Numbers In most measurements various band heads are superimposed on each other. This makes it difficult to accurately determine their respective wave numbers. This problem makes it more difficult to accurately simulate spectra. In DETEX plots, more band heads are separately visible because of the resolution of both the excitation and detection wave number. One can simply choose the most suitable Δv -band to determine its wave number.

Different detection bands can be used to determine wave numbers of band heads with low intensity that are super positioned on the rotational structure of a transition with high intensity. In this section the wave numbers of the 4-4, 5-5 and 6-6 band heads will be determined. Often, absorption or emission spectra are evaluated to determine the wave number of transitions. In these spectra the rotation band heads of the different vibrational levels may overlap. This is the case for InBr. In [21] the locations of the band heads of vibrational transitions have been determined. From these evaluations it follows that in the $\Delta v = 0$ band, the 4-4, 5-5 and 6-6 transitions are superimposed on other strong transitions such as the 0-0 transition. Therefore it is difficult to determine the exact locations of these band heads. For the determination of band heads involved in superpositions, an sr-LIF experiment can be analyzed to more accurately determine the location of the band heads.

The procedure is based on evaluating the DETEX plots. The band head identification will be based on the following two factors. One is the wave number where the band head is expected according to literature. The other is the relative theoretical intensity of the emission in different Δv bands. This last aspect is used to determine in which Δv band to search. In the case of examining the 4-4, 5-5 and 6-6 transition of InBr this is the $\Delta v = 2$ band. The relative intensity of the different bands is also used to identify peaks. The intensity detected in Δv band depends on the population of the upper level and the Franck-Condon factor of the transition. The population of the upper level is created by absorption. The population of the upper level therefore depends on the Franck-Condon factor for the excitation and on the population of the lower level. An illustration of the basic principles behind the method is presented in figure (21).

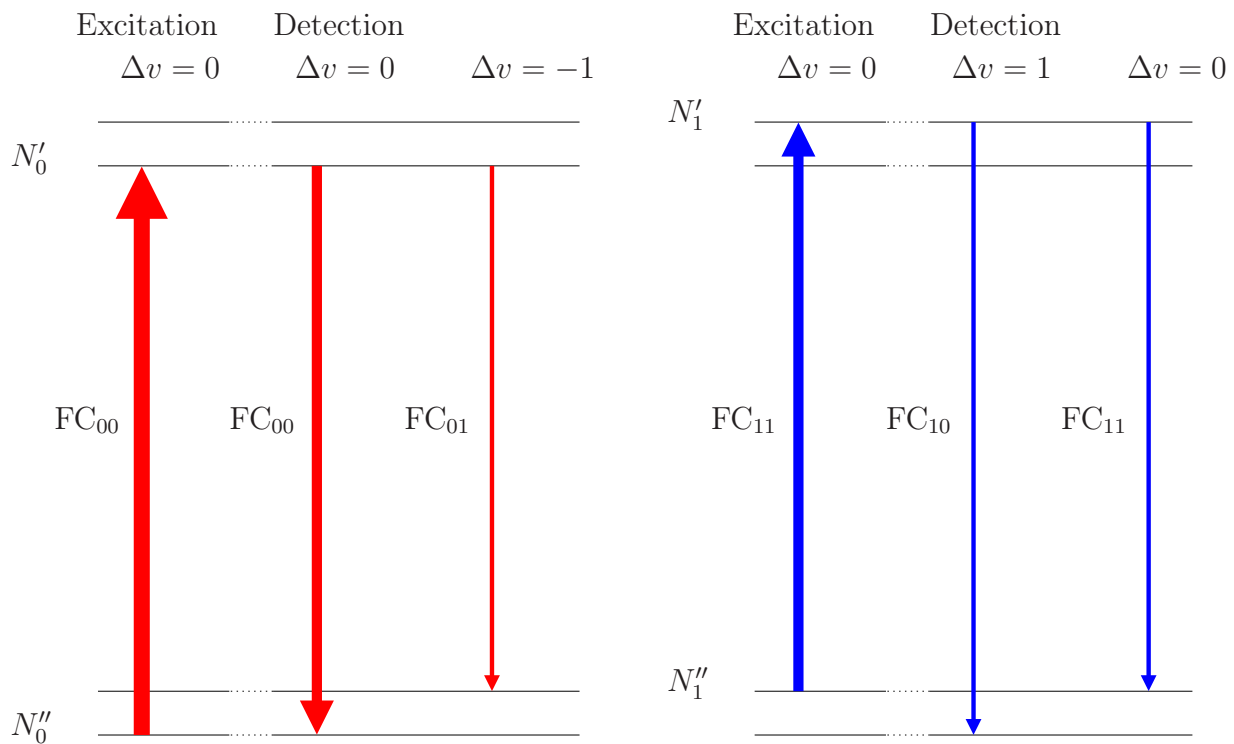


Figure 21. The intensity detected in Δv band depends on the population of the upper level and the Franck-Condon factor of the transition, indicated in the figure as FC_{xy} , where x denotes v_{upper} and y v_{lower} . The population of the upper level depends on the Franck-Condon factor in the excitation and the population of the lower level. The fluorescence from upper level vibration 0 to lower level vibration 0 is more intense than the fluorescence from upper level 1 to lower level 1. In the spectrum, these transitions are superimposed in the $\Delta v = 0$ band, and therefore it is difficult to identify the properties of the 1-1 transition. In the $\Delta v = 1$ band, there is no emission from the upper level vibration 0, therefore it is easier to identify emission from upper level vibration 1 in this band.

Vibrational level 0 as well as vibrational level 1 of the excited A-state have no emission in the $\Delta v = 2$ band. Therefore, after excitation in $\Delta v = 0$, the emission in the $\Delta v = 2$ band is evaluated. Upper level 4 has emission in this band; the 4-2 transition

does emit in this band. Vibration levels 2 and 3 of the A-state may also have emission in the $\Delta v = 2$ band, however the Franck-Condon factors of the 2-2 and 3-3 transitions are very small. This means that the vibration levels 2 and 3 of the A-state will have a very small population, therefore the 2-0 and 3-1 transition in the $\Delta v = 2$ band are not expected to be strong.

Although on the detection axis, the wave number of the 4-2 transition is shown, the wave number on the excitation axis is the wave number at which the 4-4 excitation has taken place, hence the band head of the 4-4 transition can be determined without being troubled by light from the 0 and 1 upper vibration level. The 4-2 transition can also be determined from a normal absorption or emission experiment, but in normal absorption or emission experiments it does not yield information about the 4-4 transition. Also for the 5-5 and the 6-6 transition, the $\Delta v = 2$ band can be evaluated.

In table (11), the predicted relative intensities of the peaks¶ detected in the the $\Delta v = 2$ band are listed. Although all the information on intensities is available from

Table 11. The relative intensities of emission in the $\Delta v = 2$ band depending on the upper level v' , after excitation in the $\Delta v = 0$ band. The data is scaled to a value of 1 for the emission of upper level 0 in the $\Delta v = 0$ band.

transition	relative intensity
$v' = 0 \rightarrow v'' = -2$	-
$v' = 1 \rightarrow v'' = -1$	-
$v' = 2 \rightarrow v'' = 0$	0.001
$v' = 3 \rightarrow v'' = 1$	0.001
$v' = 4 \rightarrow v'' = 2$	0.007
$v' = 5 \rightarrow v'' = 3$	0.014
$v' = 6 \rightarrow v'' = 4$	0.016
$v' = 7 \rightarrow v'' = 5$	0.014
$v' = 8 \rightarrow v'' = 6$	0.011

the DETEX plots, it is difficult to visualize the intensity profile from them. Therefore, the part of the DETEX plot that shows the $\Delta v = 2$ band is spectrally integrated. The resulting partial spectrum shows the intensity of emission in the $\Delta v = 2$ band after absorption in the $\Delta v = 0$ band as a function of the wave number of absorption. The result is shown in figure 22. In table 12 the wave number of the identified band heads is displayed.

When sr-LIF measurements are partially integrated, they give spectra like the ones in figure (22). This type of spectra can be made for detection in different Δv bands.

By making the right choice of excitation and detection bands, the signal from the desired upper level can be found with as little as possible interference from other transitions. Therefore the wave numbers of the transitions involved in superposition in

¶ scaled to an intensity of 1 for the emission of upper level 0 in the $\Delta v = 0$ band

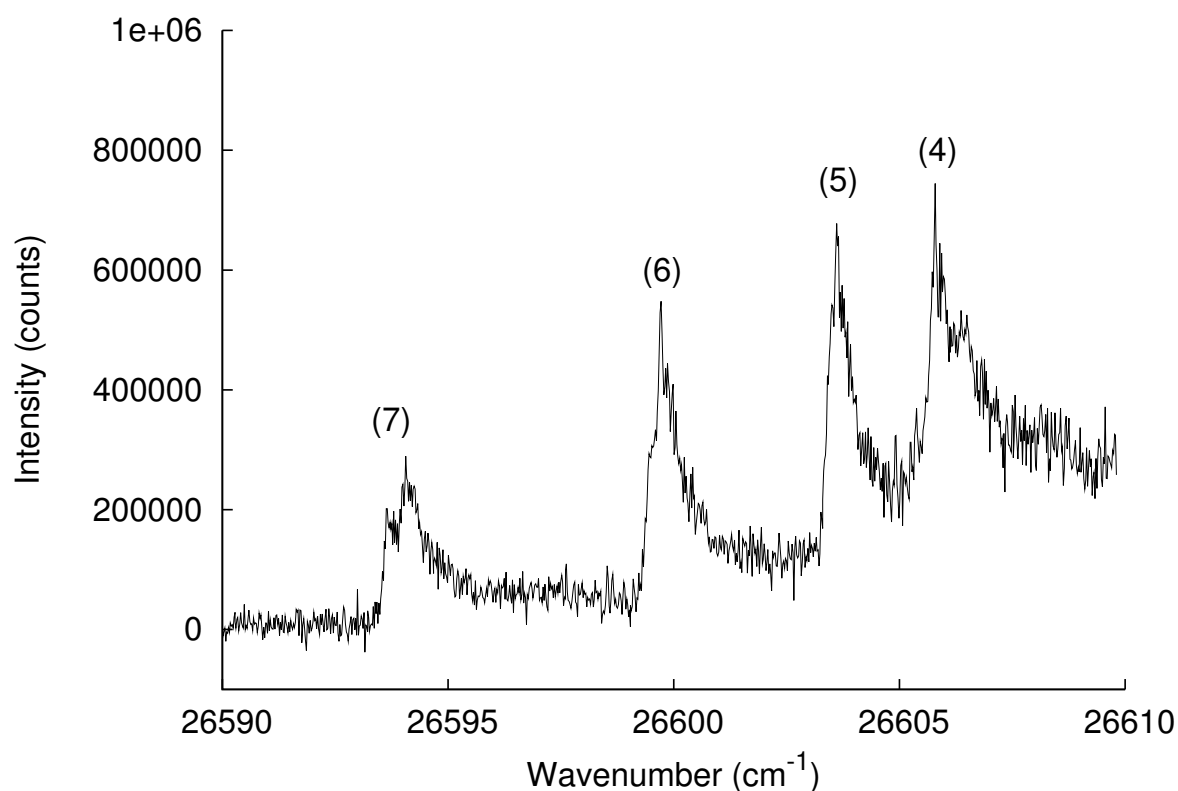


Figure 22. The intensity of emission in the $\Delta v = 2$ band after absorption in the $\Delta v = 0$ band, as a function of the wave number of absorption. The number indicates the vibration level of the upper state.

Table 12. The wave number of the band heads of the $\Delta v = 0$ absorption spectrum. A systematic error resulting from a shift of the excitation axis as a whole should be taken into account on top of the error indicated in the table.

v'	wavenumber (cm^{-1})	[21] (cm^{-1})	difference (cm^{-1})
4	26605.77 ± 0.07	26605.47	0.30
5	26603.59 ± 0.06	26603.78	-0.19
6	26599.70 ± 0.04	26599.66	0.04
7	26593.65 ± 0.06	26593.61	0.04
0	26599.00 ± 0.04	26599.00	0.00

a normal absorption or emission experiment, can be more accurately determined from a sr-LIF experiment.

In this section a calculation has been made to calculate the intensities emitted by the different upper levels in the different Δv bands based on the Franck-Condon factors. The other way around, this principle can be used to calculate Franck-Condon factors based on the relative intensities of the different upper levels in integrated spectra of the different Δv bands. This is because by comparing the shape of the different integrated spectra insight can be gained on the contributions of other upper levels and the effect

of redistribution.

5.2. InBr Vapor with Background Gas

Spectrally resolved measurements were also performed for the $\Delta v = 0$ excitation transition in InBr vapor with 2.5 mbar as a background gas, but without plasma. Figure 23 shows the DETEX plot obtained from measurements.

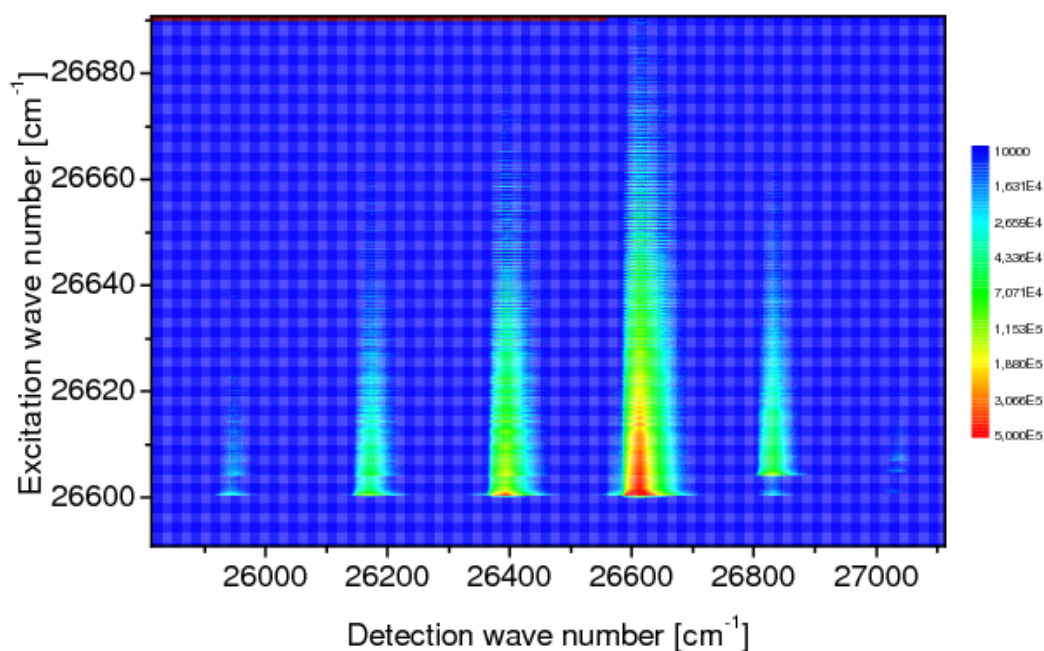


Figure 23. The DETEX plot of the sr-LIF measurement on InBr with 2.5 mbar of Argon as a background gas. Excitation was in the $\Delta v = 0$ band. From left to right the bands $\Delta v = -3$ through $\Delta v = +2$ are shown. The vibrational bands do not show a separation into rotational branches as opposed to the DETEX plot obtained without the background gas.

Comparing this DETEX plot with the DETEX plot of the tube without the background gas, it is observed that the vibrational bands look very different when the background gas is present. The rotational branches are not visible anymore; each vibrational band is now represented by a very wide, unresolved spectrum.

From this it is concluded that the rotational redistribution processes⁺ are much faster than the optical decay processes. The overall species density in the tube is higher due to the presence of the Argon. The rotational redistribution visible in figure 23 is caused by the collisions with Argon.

Rotational branches are not visible anymore, but vibrational bands are still clearly visible. The intensity ratios of these vibrational bands appear about the same as in

⁺ *i.e.* the processes that redistribute the excited molecules over all the rotational levels in the excitation space of InBr. In other words, the processes that thermalize the distribution over all rotational states.

the DETEX plot of the tube without the background gas. To confirm this, the relative intensities of the different vibrational bands were determined, in exactly the same way as in the previous section and they confirm that no vibrational redistribution has occurred.

The relative intensities of the various Δv -bands at 26600 cm^{-1} for the determination of the Franck-Condon factors are listed in table 13.

Table 13. Franck-Condon factors determined from the DETEX plots compared with the relative intensities in the presence of a buffergas.

	InBr vapor	InBr vapor + Argon
$\Delta v = +2$	0.001	0.000
$\Delta v = +1$	0.003	0.009
$\Delta v = 0$	0.602	0.621
$\Delta v = -1$	0.289	0.267
$\Delta v = -2$	0.088	0.084
$\Delta v = -3$	0.018	0.019

5.3. Capacitively Coupled Plasma

The measurements discussed in this section were performed with the same tube as in the previous section, containing InBr powder and Argon at a pressure of 2.5 mbar. To make a plasma, the RF amplifier discussed in section 3 was used at 13.56 MHz. It was connected to the tube via an L-type matching network. The measurements were performed with the RF power set to 15 W. The effect of the plasma on the cold spot temperature was negligible.

To allow the plasma to stabilize, measurements were started at least 1 hour after the start of the plasma. All other settings of the trigger system, the laser and the camera used to perform these experiments were identical to the experiment in the previous section.

The DETEX plot obtained from a burning plasma is shown in figure 24.

Comparing figure 24 and figure 23 reveals no significant differences. From this it is concluded that for these conditions, the impact of the plasma on the fluorescence processes is very small, *i.e.* below the detection limit of our setup.

5.4. Inductively Coupled Plasma

For studies of the InBr plasma lamp, the first step was to find out at what locations in the lamp LIF-experiments are possible.

The most suitable location was picked and a DETEX plot was made for this location. No LIF-signal could be observed in the center of the lamp, but in other sections of the lamp the LIF-signal could be observed. These sections were just outside the bright center of the lamp, at the point where the white color faded to blue.

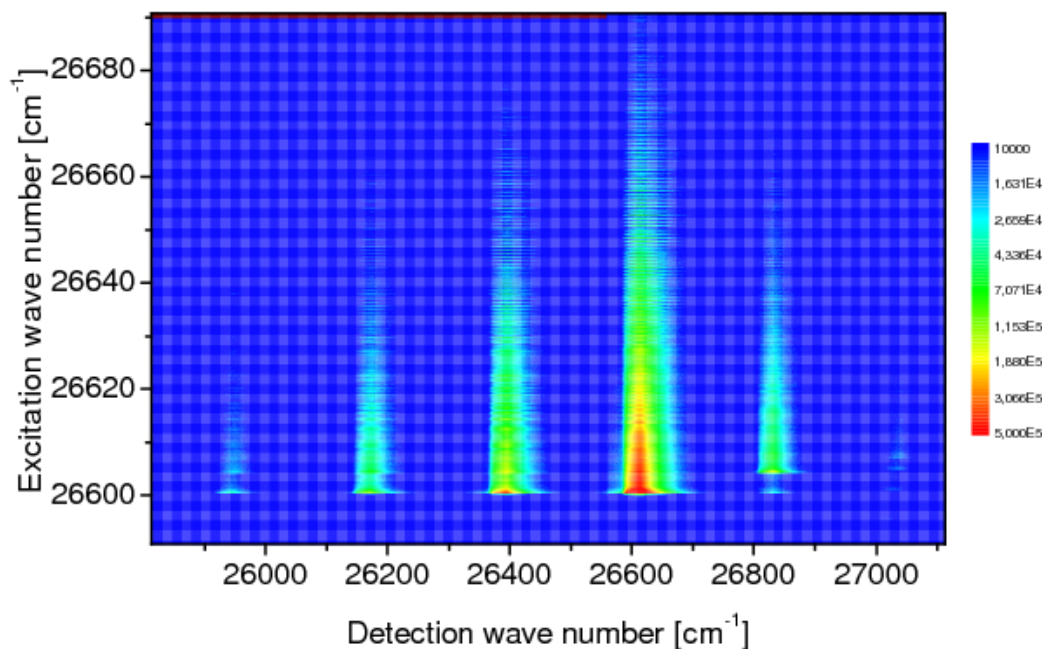


Figure 24. The DETEX plot of the sr-LIF measurement on a tube with a plasma of InBr with 2.5 mbar of Argon as a background gas. Excitation was in the $\Delta v = 0$ band. From left to right the bands $\Delta v = -3$ through $\Delta v = +2$ are shown. The vibrational bands do not show a separation into rotational branches as opposed to the DETEX plot obtained without the background gas.

This fact that no LIF signal could be observed in the center of the lamp leads to the question whether the LIF-signal was actually not there, or just not visible because the lamp masked the fluorescence by its own emissions. To gain insight in this matter, the intensity fluctuations of the plasma emission in the center of the lamp was compared to the intensity of the fluorescence signal at the sections where it could be observed. This comparison gave rise to the conclusion that the LIF signal is in fact not present at the center of the lamp. If it were there, it would have been observed, since the fluorescence signal elsewhere in the lamp exceeds the fluctuations of the plasma by a factor ~ 5 .

From this the conclusion is drawn that all the InBr in the center of the lamp is completely dissociated, so all molecular contributions to the spectrum originate from the edge of the plasma, where (3-particle) association processes can compete with the dissociation process, due to the lower plasma density. This also explains the strong atomic character of an inductive InBr lamp.

A DETEX plot was created for the section of the lamp where the LIF signal could be observed. Figure 25 shows this plot.

The uninterrupted diagonal line in the DETEX plot is an interesting artefact. It is caused by scattered light from the laser and therefore this line indicates the position where the detection wave number is equal to the excitation wave number.

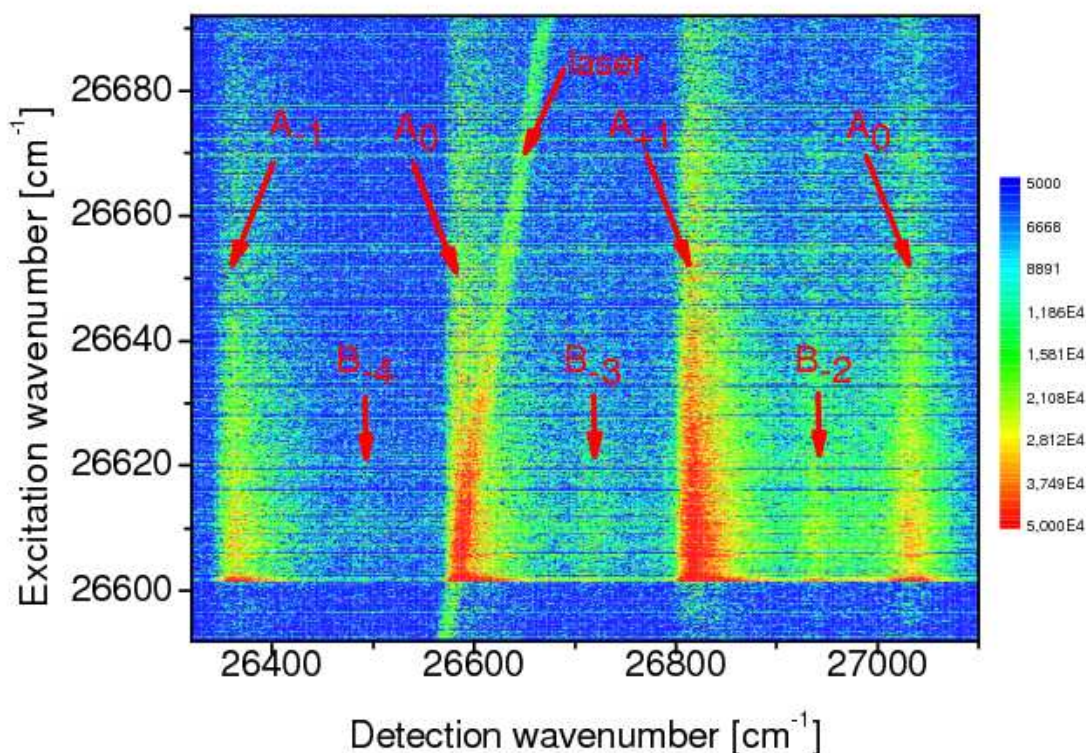


Figure 25. The DETEX plot for the **the edge of the** InBr inductively coupled plasma lamp. From left to right the $\Delta v = -1$ through $\Delta v = +2$ vibrational bands of the A-state are visible and some (faint) B-state bands. They are marked in the graph where *e.g.* A₋₂ stands for the $\Delta v = -2$ band of the A-state. Another striking feature of this DETEX plot is the diagonal line that runs through the $\Delta v = 0$ band of the A-state. This is scattered light from the laser. Its presence means that it is difficult to get accurate intensity data from this plot, however it is unavoidable and gives a good visual reference for the excitation frequency.

Another important observation is that all transitions, both A-X and B-X transitions, start at the same excitation wave number. This is different from what was observed in all other measurements. It indicates that in this situation, *vibrational* redistribution plays an important role. Furthermore, it is noted that the A-X emission at $\Delta v = +1$ is more intense than the emission at $\Delta v = 0$. This is an unexpected result as well, because the excitation of the laser produces population in $v' = 0$. Somehow, more fluorescence appears at photon energies higher than the energy of the photons supplied for excitation by the laser.

Similar to the measurements with the background gas, the rotational splitting is no longer visible, which is unsurprising.

The most important observation though, is that emission from the B-state occurs when excitation is to the A-state. This means that somehow, molecules are transferred from the A-state to the B-state. The emission seen in the B-bands is not just plasma

emission, as it is not present when the laser energy is lower than $\sim 26600 \text{ cm}^{-1}$ —and thus no laser excitation of the A-state takes place— but it is also clear that just the presence of the laser beam itself is not enough to create the emission from the B-state from the same observation.

It cannot be determined exactly how population is transferred to the B-state. Direct collisional transfer cannot be ruled out and neither can increased plasma emission due to increased population of the A-state.

6. Conclusions

For the correct assignment and interpretation of rovibronic spectra, sr-LIF measurements have a great advantage compared to normal emission or absorption spectra. This advantage is that there is a wave number axis for both the emission wave number as well as for the absorption wave number in the resulting DETEX plot. Normal emission or absorption spectra only have one of the two. The newly introduced DETEX plot is a very insightful way of representing the data found with this measuring technique. It also enables exploration of finer details of molecular spectra.

In a DETEX plot, transitions that interfere with each other in a normal absorption or emission spectrum can be separated. This splitting may occur for rotational transitions as well as for vibration transitions. Due to this splitting, in a DETEX plot, transitions with a low intensity can be studied with less interference from other transitions with higher intensity.

In this article, the splitting of rotational branches has been used to extend a list produced by [23], containing the wave numbers at which the rotational transition of the electronic A-state vibrational level 0 to the ground state vibrational level 0 of InBr occurs. Almost 30 extra P-branch transitions have been identified.

The list of wave numbers of rotational transitions that was found to expand the list in [23] has been used to determine the rotational constant of $v = 0$ of the A-state and its anharmonicity, B_{A0} .

For the transition from $v = 1$ of the A-state to $v = 0$ of the ground state, a list of wave numbers of rotational transitions was also produced by looking at the DETEX plot for excitation via the $\Delta v = +1$ band. This list is incomplete, *i.e.* the beginning is missing. To still assign the correct rotational quantum number J to the transitions found, comparisons to the known values of such as B_{A0} were made. After this assignment, the value of the rotational constant B_{A1} of the $v = 1$ level of the A-state and its anharmonicity were determined. Similarly, B_{X1} and its anharmonicity were determined. The constants determined from all these experiments are listed in table 14. The values found and the branch that has the band head are in agreement with the fact that $B' > B''$ as was expected in section 2.

Franck-Condon factors for vibrational transitions from $v = 0$ and $v = 1$ of the A-state of InBr to the ground state were determined by comparing the intensities of the various vibrational bands in the appropriate DETEX plots.

Table 14. Rotational constants and anharmonicities determined in this work.

constant	value
B_{A0}	$0.058410 \pm 0.000002 \text{ cm}^{-1}$
D_{A0}	$1.59 \cdot 10^{-8} \pm 0.01 \cdot 10^{-8} \text{ cm}^{-1}$
B_{A1}	$0.05809 \pm 0.00005 \text{ cm}^{-1}$
D_{A1}	$1.8 \cdot 10^{-8} \pm 0.2 \cdot 10^{-8} \text{ cm}^{-1}$
B_{X1}	$0.056677 \pm 0.00002 \text{ cm}^{-1}$
D_{X1}	$2.83 \cdot 10^{-8} \pm 0.01 \cdot 10^{-8} \text{ cm}^{-1}$

In this work, the splitting of vibrational transitions has been used to determine the wave number at which the band heads of the 4-4, 5-5 and 6-6 vibrational transition between the electronic A-state and the ground state of InBr occur. In a normal absorption or emission spectrum the much stronger 0-0 transition is located in the same wave number range. This makes the determination of the location of the 4-4, 5-5 and 6-6 band head nearly impossible or inaccurate at best without the DETEX plots.

In the DETEX plot, the $\Delta v = +2$ band emission has been used to determine at which wave number emission from vibrational levels 4, 5 and 6 of the electronic A-state occur. Since the excitation of InBr has been in the $\Delta v = 0$ band, the wave number on the excitation axis can be used to determine the band heads of the 4-4, 5-5 and 6-6 vibrational transitions.

Also, DETEX plots were made of not just the InBr vapor, but vapor in combination with a background gas, of 2.5 mbar of Argon. In this situation, rotational redistribution due to the increased collision rate was shown to be significant compared to optical relaxation. This redistribution obscured the rotational branches, transforming each Δv band into a single smeared out shape.

Additionally, a capacitively coupled plasma was produced in the tube with InBr and Argon at a power of ~ 10 W. The capacitively couples plasma yielded similar data in a DETEX plot.

When a LIF experiment was attempted for an inductively coupled plasma, no LIF signal was visible in the center of the discharge. From this observation, the conclusion is that all the InBr in the center of the lamp is completely dissociated. All molecular contributions to the spectrum originate from the edge of the plasma, where association processes can compete with the dissociation process, due to the lower plasma density. The high degree of dissociation also explains the strong atomic character of an inductive InBr lamp. **It was, however, possible to detect the LIF signal on the edge of the plasma in an inductively coupled discharge.**

7. References

- [1] G. G. Lister, J. E. Lawler, W. P. Lapatovich, and V. A. Godyak. The physics of discharge lamps. *Rev. Mod. Phys.*, 76(2):541–598, Jun 2004.

- [2] John F. Waymouth. *Electric discharge lamps*. Monographs in modern electrical technology. M.I.T. Press, Cambridge, Mass, 1971.
- [3] Cees Ronda. *Luminescence*. Wiley-VCH, Weinheim, 2008.
- [4] W. W. Stoffels, T. Nimalasuriya, A. J. Flikweert, and H. C. J. Mulders. Discharges for lighting. *Plasma Physics and Controlled Fusion*, 49:505–507, December 2007.
- [5] Scholl et.al. Low pressure gas discharge lamp with a mercury-free gas filling. 2004. US6731070B2.
- [6] Scholl et.al. Low pressure gas discharge lamp with gas filling containing tin. US2005/0242737A1.
- [7] Hilbig et.al. Low-pressure gas discharge lamp with an alkaline earth chalcogenides as electron emitter material. US2006/0214590A1.
- [8] Hildenbrand et.al. Low pressure vapor discharge lamp with a mercury-free gas filling. US2007/0132360A1.
- [9] J. W. Hastie. *High temperature vapors : science and technology*. Materials science and technology. Academic Press, New York, 1975.
- [10] E. Schnedler. The calculation of complex chemical equilibria. *CALPHAD*, 8(3):265–279, 1984.
- [11] M. Bruchhausen, J. Voigt, T. Doerk, S. Hädrich, and J. Uhlenbusch. Resonant coherent anti-stokes raman scattering applied to vapor phase ini. *Journal of Molecular Spectroscopy*, 201:70–82, 2000.
- [12] R. Hilbig, A. Koerber, J. Baier, and R. Scholl. Molecular discharges as light sources. In G. Zissis, editor, *Proceedings of the 10th International Symposium on the Science and Technology of Light Sources*, number 182 in Conference Series, pages 75–84, Bristol and Philadelphia, 2004. IoP.
- [13] R. Hilbig, A. Koerber, D. Hayashi, S. Schwan, and R. Scholl. Investigations on low pressure indium mono-halide discharges. In M.Q. Liu and R. Devonshire, editors, *Proceedings of the 11th International Symposium on the Science and Technology of Light Sources*, pages 423–424, Sheffield, 2007. FAST-LS Ltd.
- [14] Peter Flesch. *Light and Light Sources*. Springer-Verlag, Berlin, 2006.
- [15] Dušan Papoušek. *Vibration-rotational spectroscopy and molecular dynamics: advances in quantum chemical and spectroscopical studies of molecular structures and dynamics*. Volume 9 of Advanced series in physical chemistry. World Scientific, Singapore, 1997.
- [16] David J. Griffiths. *Introduction to Quantum Mechanics*. Prentice-Hall, inc., Englewood Cliffs, N.J., 1984.
- [17] Marcelo Alonso and Edward J. Finn. *Quantumfysica*. Fundamentele Natuurkunde. Delta Press BV, Overberg, 1994.
- [18] I. Kovacs. *Rotational structure in the spectra of diatomic molecules*. 1969.
- [19] E. E. Whiting, A. Schadee, J. B. Tatum, J. T. Hougen, and R. W. Nicholls. Recommended conventions for defining transition moments and intensity factors in diatomic molecular spectra. *J. Mol. Spectrosc.*, 80, 1980.
- [20] G. Herzberg. *Molecular Spectra and Molecular Structure*. Vol. 1 Spectra of Diatomic Molecules. D. van Nostrand company, Inc., Princeton, New Jersey, second edition 1950.
- [21] V.B.Singh, A.K.Rai, S.B.Rai, and D.K.Rai. Studies in the A-X and B-X system of InBr. *Indian J. Phys*, 62B, 1988.
- [22] Xinzhen Yang, Meirong Lin, Wenli Zou, Yunjing Li, and Baozheng Zhang. Experimental and theoretical study on the electronic states and spectra of inbr. *Phys. Chem. Chem. Phys*, 5:4786–4789, 2003.
- [23] S. Vempatie and W. Jones. Rotational analysis of the $A0^+ - X0^+$ systems of indium bromide. *J. Mol. Spectrosc.*, 119, 1986.
- [24] S. K. Mishra, Raj K. S. Yadav, V. B. Singh, and S. B. Rai. Spectroscopic studies of diatomic indium halides. *J. Phys. Chem. Ref. Data*, 33(2), 2004.
- [25] J. Franck. Elementary processes of photochemical reactions. *Transactions of the Faraday Society*, 21, 1926.
- [26] Edward Condon. A theory of intensity distribution in band systems. *Phys. Rev.*, 28(6):1182–1201, Dec 1926.

- [27] P. W. Atkins. *Physical Chemistry*. University Press, Oxford, UK, sixth edition 1999.
- [28] Wolfgang Demtröder. *Laser Spectroscopy*. Springer, 2002.
- [29] Yasuhiko Hirana, Yasuhiko Tanaka, Yasuro Niidome, and Naotoshi Nakashima. Strong micro-dielectric environment effect on the band gaps of (n,m)single-walled carbon nanotubes. *Journal of the American Chemical Society*, 132(37):13072–13077, 2010.